Statistical Regularization for TomoSAR Imaging With Multiple Polarimetric Observations

Gustavo Daniel Martín-del-Campo-Becerra [ID], Eduardo Torres-García [ID], Deni Librado Torres-Román [ID], Sergio Alejandro Serafín-García [ID], and Andreas Reigber [ID], *Fellow, IEEE*

Abstract—The polarimetric versions of focusing techniques for synthetic aperture radar (SAR) tomography (TomoSAR), apart from estimating the pseudopower and retrieving the height of reflectors from the recovered local maxima, allow extracting the associated scattering mechanisms. Additionally, scattering patterns can be examined by means of polarimetric indicators like alpha mean angle, used to associate observables with physical properties of the medium. Aimed at easing the analysis of the scattering processes occurring in the illuminated scene, this article extends the weighted covariance fitting (WCF) based iterative spectral estimator (WISE) to the polarimetric configuration, called hereafter PolWISE. The addressed technique attains finer resolution than conventional methods like PolCapon, performing suppression of artefacts and ambiguity reduction. PolWISE is a statistical regularization approach, which reduces the TomoSAR inverse problem to the selection of a regularization parameter, chosen via the L-Curve method. Furthermore, being PolWISE an iterative technique, under/over regularization is prevented by terminating the procedure at an appropriate iteration. A stopping rule based on Kullback–Leibler information criterion is employed. The PolWISE algorithm is assessed thoroughly through simulations and experiments on fully polarimetric TomoSAR airborne data at L-band, acquired from an urban scenario.

Index Terms—Polarimetric synthetic aperture radar (PolSAR), SAR tomography (TomoSAR), statistical regularization, weighted covariance fitting (WCF).

NOMENCLATURE

A. List of Acronyms

AIC	Akaike information criterion.
BIC	Bayesian information criterion.
DR	Detection rate.
EDC	Efficient detection criterion.
KL	Kullback–Leibler.
InSAR	Interferometric SAR.
JPL	Jet propulsion laboratory.
LOS	Line-of-sight.
ML	Maximum likelihood.
MO	Model order.
MSF	Matched spatial filtering.
MUSIC	Multiple signal classification.
NASA	National aeronautics and space administration.
pdf	Probability density function.
PolSAR	Polarimetric SAR.
PLOS	Perpendicular to the LOS.
PSP	Power spectrum pattern.
RMSE	Root mean square error.
ROI	Region of interest.
SAR	Synthetic aperture radar.
SLC	Single look complex.
SNR	Signal-to-noise ratio.
TomoSAR	SAR tomography.
UAVSAR	Uninhabited aerial vehicle SAR.
WCF	Weighted covariance fitting.
WISE	WCF-based iterative spectral estimator.

B. Glossary of Notation

$\langle \cdot \rangle$	Averaging operator.
$\mathbf{D}(\mathbf{x})$	Diagonal matrix with vector $\mathbf{x}$ at the main diagonal.
$\text{eigen}\{\cdot\}$	Eigen decomposition.
$\|\cdot\|$	Euclidean ℓ_2-norm.
$E(\ )$	Expectation operator.
$\odot$	Hadamard product.
$^+$	Hermitian conjugate (adjoin).
$\mathbf{I}$	Identity matrix.
$\{\mathbf{U}\}_{\text{diag}}$	Main diagonal of matrix $\mathbf{U}$.
$\ln\{\cdot\}$	Natural logarithm.
$^{\text{T}}$	Transpose.
$\text{tr}\{\mathbf{X}\}$	Trace of matrix $\mathbf{X}$.

I. INTRODUCTION

TWO main limitations arise when analyzing conventional synthetic aperture radar (SAR) imagery. On one hand, the superposition of different scattering contributions, sharing the same resolution cell, cannot be determined, since only the total backscattering is measured. On the other hand, the height of reflectors is unknown, since the elevation angle cannot be retrieved, as the SAR geometry is symmetric in elevation. These limitations are tackled via two extensions of conventional SAR: Polarimetric SAR (PolSAR) and interferometric SAR (InSAR), respectively. Taking advantage of contributions from different
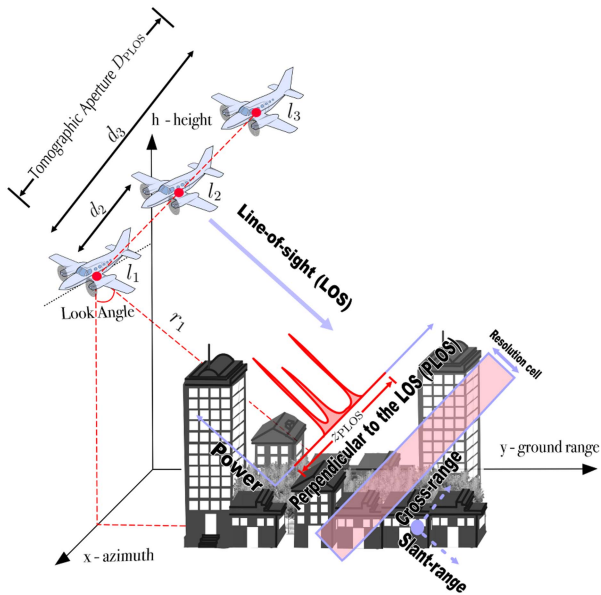
Fig. 1.   TomoSAR acquisition geometry using parallel passes (not to scale).

polarimetric channels, PolSAR [1], [2] permits discriminating the different types of scattering mechanisms and examining the physics of reflection processes. Whereas InSAR [3], [4] is capable of generating high resolution digital elevation models by analyzing the phase difference between two SAR images, acquired at slightly different positions.

More recently, aimed at producing three-dimensional imagery of the illuminated scene and solving the layover problem, SAR tomography (TomoSAR) was introduced [5]. As seen in Fig. 1, by acquiring several SAR images at different line-of-sight (LOS), an aperture in elevation is generated (so-called tomographic aperture). Then, exploiting antenna array theory, as done for SAR systems, a resolution in the perpendicular to the LOS (PLOS) is defined.

While fusing InSAR and PolSAR permits determining the vertical location of scattering mechanisms [6], combining TomoSAR and PolSAR allows determining how energy distributes over space, locating the radiating (backscattering) sources and extracting the associated scattering mechanisms. Moreover, the height of reflectors is recovered from the local maxima along the estimated power spectrum pattern (PSP).

By generalizing the TomoSAR signal model to the fully polarimetric configuration, conventional focusing techniques like matched spatial filtering (MSF), Capon, and multiple signal classification (MUSIC) can be adapted to the polarimetric case [7]. Making use of same signal model, this article extends the super-resolution method weighted covariance fitting (WCF) based iterative spectral estimator (WISE) [8] to the polarimetric configuration, called hereafter PolWISE. The main goal is easing both the discrimination of the different types of scattering mechanisms and the analysis of the scattering processes occurring in the illuminated scene.

PolWISE attains super-resolution, performing suppression of artefacts and ambiguity reduction. It can be understood as a postprocessing step for the enhancement of TomoSAR imagery recovered using conventional focusing techniques. The retrievals of methods like PolMSF, PolCapon, or PolMUSIC act as first input (zero iteration) to the PolWISE iterative procedure, which seeks converging into a unique solution.

PolWISE poses two particular challenges as follows.

1) Being a statistical regularization approach, PolWISE reduces the TomoSAR inverse problem to the selection of a regularization parameter, whose correct setting assures retrieving good-fitted solutions. Aimed at properly selecting such regularization parameter, the L-Curve method [9], [10] is refactored to work exclusively with data covariance matrices, since the scattering vector may not be always available, especially when not working at full resolution. Manipulations previously done to the data covariance matrix (e.g., presumming) must be equivalent in the scattering vector, which may not be at all times feasible.

2) Being PolWISE an iterative technique, over/under regularization is prevented by terminating the procedure at an appropriate iteration. Specifically, the iterative approach is terminated after reaching a solution that maximizes the Kullback–Leibler (KL) information function [11], [12] via minimizing akaike information criterion (AIC), bayesian information criterion (BIC), or efficient detection criterion (EDC).

The novel strategy is assessed through simulations and on fully polarimetric TomoSAR airborne data at L-band, acquired from an urban scenario. Scattering patterns are examined in detail by using alpha mean angle [2] as polarimetric indicator.

Scattering patterns in urban scenarios are very complex [7], since a single resolution cell may gather several contributions. Particularly, the following phenomena could occur: single-bounce reflections from surfaces as building roofs and structures made out of glass, double-bounce reflections from wall-ground and tree-trunk-ground interactions, and volume reflections from trees' canopy.

The main contributions of this article are recapitulated as follows.

1) PolWISE is introduced as the polarimetric version of WISE, a super-resolution statistical regularization technique for TomoSAR imaging.

2) The L-Curve method is refactored to work exclusively with data covariance matrices, aimed at properly selecting PolWISE's regularization parameter.

3) A stopping rule based on KL information criterion is employed to terminate the PolWISE iterative procedure, preventing under/over regularization and avoiding unnecessary iterations.

4) The capabilities of PolWISE are assessed for the single, dual and full channel cases via simulations. Afterwards, tomograms are produced and scattering mechanisms are analyzed in complex urban scenes, using fully polarimetric TomoSAR airborne data.

The rest of this article is organized as follows. Section II addresses the classical TomoSAR signal model. Section III briefly

summarizes WISE. Section IV presents the extended polarimetric TomoSAR signal model. Section V introduces PolWISE. Section VI addresses the simulations performed. Section VII shows the experimental results. Finally, Section VIII concludes this article.

II. TomoSAR Signal Model

Observe Fig. 1, the TomoSAR acquisition geometry comprises L flight tracks (passes) with different LOS. Each pass produces one SAR image. After all images are collected, the ensemble of SAR imagery is coherently combined using In-SAR techniques. Coregistration is assumed independent on height. Subsequently, the spatial spectral estimation problem [13, Chapter 6] is solved by means of the L processed signals, considered from now on as a sensors array. Recall that the spatial spectral estimation problem consists on determining how energy distributes over space and where the radiating (backscattering) sources are located.

The TomoSAR inverse problem is represented via the linear equation [8], [9], [12]

$$\mathbf{y} = \mathbf{A}\mathbf{s} + \mathbf{n}, \tag{1}$$

where vector $\mathbf{y}$ gathers the processed signals of the L passes for certain azimuth-range position. Vector $\mathbf{s}$ of size M holds the corresponding reflectivity values at the PLOS elevation positions $\{z_m\}_{m=1}^{M}$. Vector $\mathbf{n}$ accounts for the additive noise. Finally, matrix $\mathbf{A}$ contains the interferometric phase information of the backscattering sources located along the PLOS elevation positions $\{z_m\}_{m=1}^{M}$, above the reference focusing plane. Matrix $\mathbf{A}$ (so-called steering matrix) comprises the steering vectors $\{\mathbf{a}(z_m)\}_{m=1}^{M}$, as defined in [8].

Vector $\mathbf{n}$ is characterized by the correlation matrix

$$\mathbf{R_n} = \mathrm{E}(\mathbf{n}\mathbf{n}^+) = N_0\,\mathbf{I}, \tag{2}$$

where N_0 is the power spectral density of the white noise power [14]. The correlation matrix of vector $\mathbf{s}$ is defined as

$$\mathbf{R_s} = \mathrm{E}(\mathbf{s}\mathbf{s}^+) = \mathbf{D}(\mathbf{b}), \tag{3}$$

where vector $\mathbf{b} = \{|s_m|^2\}_{m=1}^{M}$. Aimed at easing the mathematical developments that led to WISE [8], entries of vector $\mathbf{s}$ are assumed uncorrelated. Finally, the correlation matrix of vector $\mathbf{y}$ is given by

$$\mathbf{R_y} = \mathrm{E}(\mathbf{y}\mathbf{y}^+) = \mathbf{A}\mathbf{R_s}\mathbf{A}^+ + \mathbf{R_n}. \tag{4}$$

The sampled (measured) data covariance matrix is expressed as

$$\mathbf{Y} = \frac{1}{J}\sum_{j=1}^{J}\mathbf{y}_{(j)}\mathbf{y}_{(j)}^+, \tag{5}$$

where J indicates the number of independent realizations (looks) of the signal acquisitions. In practice, TomoSAR is customarily treated as an ergodic process, meaning that its statistical properties are deduced from a single random realization. Multilooking is achieved through the averaging of adjacent values among the set of data covariance matrices $\mathbf{Y}$, i.e., using, by instance, a Boxcar filter.

Given the data covariance matrix $\mathbf{Y}$ and the steering matrix $\mathbf{A}$, together with some prior knowledge on the problem (e.g., about the statistics of the signal and noise), the nonlinear TomoSAR inverse problem consists in estimating the second-order statistics of the reflectivity vector $\mathbf{s}$, i.e., the PSP vector $\mathbf{b}$ at the principal diagonal of matrix $\mathbf{R_s}$. The TomoSAR problem is ill-conditioned, as it does not accomplish the *uniqueness* Hadamard condition [15, Chapter 15]. The usage of $\mathbf{Y}$ for focusing, instead of utilizing vector $\mathbf{y}$, is aimed at increasing accuracy in presence of signal-dependent (multiplicative) noise and handling the multiple nondeterministic sources [15, Chapter 18].

Several nonparametric and parametric techniques are available for retrieving the PSP as part of the direction-of-arrival estimation framework [13, Chapter 6]. Imposing some form of constraints and/or making appropriate assumptions, the different focusing techniques must guarantee retrieving well-conditioned solutions to the nonlinear TomoSAR inverse problem. On one hand, nonparametric methods do not make any assumption on the covariance structure of the data. They only assume that matrix $\mathbf{A}$ is calibrated, as the functional form of vectors $\{\mathbf{a}_m\}_{m=1}^{M}$ is known [13, Chapter 6]. On the other hand, parametric methods assume a PSP composed of point-type like backscattering sources [13, Chapter 5], reducing the spatial spectral estimation problem to the problem of selecting an integer-valued parameter [so-called model order (MO)], which describes the number of source signals impinging on the sensors array [13, Appendix C].

Parametric methods include techniques like MUSIC (summarized in [12]), whereas nonparametric ones include techniques like MSF and Capon. These three approaches are the most common TomoSAR focusing techniques, widely used (among other reasons) because of their simple implementation. MSF, by instance, is defined via [8]

$$\hat{\mathbf{b}}_{\mathrm{MSF}} = \mathbf{A}^+\mathbf{Y}\mathbf{A}, \tag{6}$$

whilst Capon is given by [8]

$$\left\{\hat{b}_{\mathrm{Capon}_m} = \frac{1}{\mathbf{a}_m^+\mathbf{R_y}^{-1}\mathbf{a}_m}\right\}_{m=1}^{M}, \tag{7}$$

with $\mathbf{R_y}$ approximated via $\mathbf{Y}$ in (5).

MSF attains a resolution $\rho_{\mathrm{PLOS}} = \lambda r_1/2D_{\mathrm{PLOS}}$ (see Fig. 1) constrained to the acquisition geometry [5], [16], with λ as the carrier wavelength. Finer resolution is attained with larger tomographic aperture D_{PLOS}. Furthermore, assuming evenly distributed passes, $d = \lambda r_1/2Z_{\mathrm{PLOS}}$ defines the maximum allowed baseline to avoid ambiguities along the PLOS height range of interest Z_{PLOS} [16].

In general, Capon and MUSIC attain finer resolution and ambiguity suppression than MSF, easing the acquisition geometry constrain, as they involve an alternative inversion of the spectrum [17]. Conversely, MSF achieves better radiometric accuracy [18]. Moreover, Capon must be provided with full-rank (invertible) covariance matrices, whereas MUSIC depends on a proper MO selection [11].

III. WCF-BASED ITERATIVE SPECTRAL ESTIMATOR

WISE is a statistical regularization approach that guarantees retrieving well-conditioned solutions by incorporating known properties of the solution into the solver. The WCF optimization problem [8], [19], [20]

$$\hat{\mathbf{b}}_{\text{WCF}} = \underset{\mathbf{b}}{\text{argmin}} \left\{ \left\| \mathbf{y}^+ \mathbf{R}_{\mathbf{y}}^{-1} \mathbf{y} + \frac{\text{tr}\{\mathbf{R}_{\mathbf{y}}\}}{\text{tr}\{\mathbf{Y}\}} \right\|^2 \right\} \quad (8)$$

is solved with the standard gradient method. Accordingly, the derivative of the objective function is set to 0, yielding

$$\left\{ \mathbf{a}_m^+ \mathbf{R}_{\mathbf{y}}^{-1} \mathbf{Y} \mathbf{R}_{\mathbf{y}}^{-1} \mathbf{a}_m = \frac{1}{\text{tr}\{\mathbf{Y}\}} \mathbf{a}_m^+ \mathbf{a}_m \right\}_{m=1}^{M}. \quad (9)$$

Subsequently, the asymptotic of the filter output is defined via Capon. Multiplying both sides in (9) by the expression in (7) and performing a sequence of simple manipulations produces the solver [8]

$$\left\{ \hat{b}_{\text{WCF}_m} = \frac{\text{tr}\{\mathbf{Y}\}}{\mathbf{a}_m^+ \mathbf{a}_m} \left(\frac{\mathbf{a}_m^+ \mathbf{R}_{\mathbf{y}}^{-1} \mathbf{Y} \mathbf{R}_{\mathbf{y}}^{-1} \mathbf{a}_m}{\mathbf{a}_m^+ \mathbf{R}_{\mathbf{y}}^{-1} \mathbf{a}_m} \right) \right\}_{m=1}^{M}. \quad (10)$$

Note the dependency of (10) on matrix $\mathbf{R}_{\mathbf{y}}$, which in turn depends on two parameters, vector $\mathbf{b}$ in (3) and factor N_0 in (2).

Aimed at easing the computation of (10), subtle assumptions and modifications are done, yielding [8]

$$\left\{ \hat{b}_{\text{WISE}_m}^{[i+1]} = \frac{\text{tr}\{\mathbf{Y}\}}{\mathbf{a}_m^+ \mathbf{a}_m} \left(\mathbf{a}_m^+ \hat{\mathbf{R}}_{\mathbf{y}}^{-1} \mathbf{Y} \hat{\mathbf{R}}_{\mathbf{y}}^{-1} \mathbf{a}_m \right) \hat{b}_m^{[i]} \right\}_{m=1}^{M},$$

$$i = 0, \ldots, I. \quad (11)$$

WISE recognizes that $\{1/\mathbf{a}_m^+ \mathbf{R}_{\mathbf{y}}^{-1} \mathbf{a}_m\}_{m=1}^{M}$ is actually the PSP vector $\mathbf{b}$ [see (7)]. However, since the actual PSP is unknown, an approximation $\hat{\mathbf{b}}$ is utilized instead, both as input and to estimate matrix $\mathbf{R}_{\mathbf{y}}$ in (4). Vector $\hat{\mathbf{b}}$ can be retrieved using different focusing techniques (e.g., MSF, Capon, or MUSIC); therefore, seeking to converge into a unique solution, WISE is introduced as an iterative procedure.

Finally, factor N_0 in $\hat{\mathbf{R}}_{\mathbf{y}}$ acts as a diagonal-loading regularization parameter, which assures matrix $\hat{\mathbf{R}}_{\mathbf{y}}$ to be always invertible. Setting factor N_0 properly is key to retrieve good-fitted solutions [9], i.e., avoiding under/overfitting. On one hand, under-fitting causes the suppression of true backscattering sources, as they are taken by noise. On the other hand, overfitting causes the false occurrence of backscattering sources, as the residual variation (i.e., noise) is considered as part of the signal.

IV. POLARIMETRIC TOMOSAR SIGNAL MODEL

Extending the signal model described in Section II to the polarimetric configuration, permits adapting the abovementioned focusing techniques to the polarimetric case. In this way, apart from estimating the polarimetric PSP $\mathbf{b}_{\text{Pol}}$ and retrieving the height of reflectors from the recovered local maxima, the extraction of the associated scattering mechanisms is also possible.

For a given azimuth-range position, vector $\mathbf{y}_{\text{Pol}} \in \mathbb{C}^{P \times L}$ (with P as the number of polarization channels) is characterized by [7]

$$\mathbf{y}_{\text{Pol}} = \sum_{m=1}^{M} \sqrt{\tau_m} \boldsymbol{\eta}_m \odot \mathbf{B}(z_m) \mathbf{q} + \mathbf{n}. \quad (12)$$

The number of backscattering sources M is assumed known. The polarimetric reflectivity of the mth source is expressed as $\sqrt{\tau_m}$, whereas τ_m denotes SPAN $= |S_{hh}|^2 + |S_{hv}|^2 + |S_{vv}|^2$, with $P = 3$ and S_{xy} as the elements of the scattering (Sinclair) matrix [1], [2]. Vector $\boldsymbol{\eta}_m$ accounts for the multiplicative noise. Vector $\mathbf{q}$ of size P is a unitary reflection mechanism, such that $\mathbf{q}^+ \mathbf{q} = 1$. The absolute values of its coefficients $\{|q_p|\}_{p=1}^{P}$ indicate the relative intensities between polarizations. As before, vector $\mathbf{n}$ accounts for the additive noise. Finally, for certain PLOS elevation position z, the steering vector matrix $\mathbf{B}(z)$ of size $(P \times L) \times P$ is given by

$$\mathbf{B}(z) = \begin{bmatrix} \mathbf{a}(z) & \mathbf{0} & \mathbf{0} \\ \mathbf{0} & \mathbf{a}(z) & \mathbf{0} \\ \mathbf{0} & \mathbf{0} & \mathbf{a}(z) \end{bmatrix} \quad (13)$$

with $P = 3$.

Vectors $\{\mathbf{u}_m = \mathbf{B}(z_m)\mathbf{q}\}_{m=1}^{M}$ of size $(P \times L) \times 1$ are employed to derive the polarimetric versions of the previously addressed focusing techniques. These vectors replace the steering vectors $\{\mathbf{a}(z_m)\}_{m=1}^{M}$ utilized in the single-polarization configuration. By instance, polarimetric Capon (called PolCapon) is expressed as

$$\left\{ \hat{b}_{\text{PolCapon}_m} = \frac{1}{\mathbf{u}_m^+ \mathbf{R}_{\mathbf{y}_{\text{Pol}}}^{-1} \mathbf{u}_m} \right\}_{m=1}^{M}. \quad (14)$$

Subsequently, maximizing (14) in terms of the polarization state $\mathbf{q}$ by $\max_{\|\mathbf{q}\|=1} \{1/\mathbf{q}^+ \mathbf{B}_m^+ \mathbf{R}_{\mathbf{y}_{\text{Pol}}}^{-1} \mathbf{B}_m \mathbf{q}\}$ yields

$$\left\{ \hat{b}_{\text{PolCapon}_m} = w_{m_{\min}}^{-1} \right\}_{m=1}^{M}, \quad (15)$$

with

$$\{w_{m_p}\}_{p=1}^{P}, \quad \{\mathbf{v}_{m_p}\}_{p=1}^{P} = \text{eigen}\{\mathbf{B}_m^+ \mathbf{R}_{\mathbf{y}_{\text{Pol}}}^{-1} \mathbf{B}_m\}. \quad (16)$$

Matrix $\mathbf{R}_{\mathbf{y}_{\text{Pol}}} = \text{E}(\mathbf{y}_{\text{Pol}} \mathbf{y}_{\text{Pol}}^+)$ is approximated via $\mathbf{Y}_{\text{Pol}}$ of size $(P \times L) \times (P \times L)$, computed in a similar manner as in (5). Value $w_{m_{\min}}$ corresponds to the minimum eigenvalue; whereas, $\mathbf{v}_{m_{\min}}$ is the associated eigenvector. Eigenvector $\mathbf{v}_{m_{\min}}$ is regarded as a polarimetric reflection mechanism, which allows determining the physical characteristics of the target [7]. It specifies optimum polarimetric combinations according to Capon. The polarimetric PSP is recovered via (15), while its local maxima point out the height of reflectors.

V. POLARIMETRIC WISE

This section extends WISE in (11) to the polarimetric configuration. As done with PolCapon in Section IV, steering vectors $\{\mathbf{a}(z_m)\}_{m=1}^{M}$ in (10) are replaced with vectors $\{\mathbf{u}_m = \mathbf{B}(z_m)\mathbf{q}\}_{m=1}^{M}$, resulting in

$$\left\{ \hat{b}_{\text{WCF}_m} = \frac{\text{tr}\{\mathbf{Y}_{\text{Pol}}\}}{\mathbf{u}_m^+ \mathbf{u}_m} \left(\frac{\mathbf{u}_m^+ \mathbf{R}_{\mathbf{y}_{\text{Pol}}}^{-1} \mathbf{Y}_{\text{Pol}} \mathbf{R}_{\mathbf{y}_{\text{Pol}}}^{-1} \mathbf{u}_m}{\mathbf{u}_m^+ \mathbf{R}_{\mathbf{y}_{\text{Pol}}}^{-1} \mathbf{u}_m} \right) \right\}_{m=1}^{M}. \quad (17)$$

Afterwards, maximizing (17) in terms of the polarization state $\mathbf{q}$ by

$$\max_{\|\mathbf{q}\|=1}\left\{\frac{\mathrm{tr}\left\{\mathbf{Y}_{\mathrm{Pol}}\right\}}{\mathbf{q}^{+}\mathbf{B}_{m}^{+}\mathbf{B}_{m}\mathbf{q}}\left(\frac{\mathbf{q}^{+}\mathbf{B}_{m}^{+}\mathbf{R}_{\mathbf{y}_{\mathrm{Pol}}}^{-1}\mathbf{Y}_{\mathrm{Pol}}\mathbf{R}_{\mathbf{y}_{\mathrm{Pol}}}^{-1}\mathbf{B}_{m}\mathbf{q}}{\mathbf{q}^{+}\mathbf{B}_{m}^{+}\mathbf{R}_{\mathbf{y}_{\mathrm{Pol}}}^{-1}\mathbf{B}_{m}\mathbf{q}}\right)\right\} \tag{18}$$

produces

$$\left\{\hat{b}_{\mathrm{WCF}m}=\frac{\mathrm{tr}\left\{\mathbf{Y}_{\mathrm{Pol}}\right\}}{\mathbf{B}_{m}^{+}\mathbf{B}_{m}}\,w_{m_{\max}}\right\}_{m=1}^{M}, \tag{19}$$

with

$$\left\{w_{m_{p}}\right\}_{p=1}^{P},\quad\left\{\mathbf{v}_{m_{p}}\right\}_{p=1}^{P}$$

$$=\mathrm{eigen}\left\{\frac{\mathbf{B}_{m}^{+}\mathbf{R}_{\mathbf{y}_{\mathrm{Pol}}}^{-1}\mathbf{Y}_{\mathrm{Pol}}\mathbf{R}_{\mathbf{y}_{\mathrm{Pol}}}^{-1}\mathbf{B}_{m}}{\mathbf{B}_{m}^{+}\mathbf{R}_{\mathbf{y}_{\mathrm{Pol}}}^{-1}\mathbf{B}_{m}}\right\}. \tag{20}$$

Value $w_{m_{\max}}$ refers to the maximum eigenvalue; whereas, $\mathbf{v}_{m_{\max}}$ is the associated eigenvector. Vector $\mathbf{v}_{m_{\max}}$ is regarded as a polarimetric reflection mechanism, which specifies optimum polarimetric combinations in sense of WCF.

PolWISE performs subtle assumptions and modifications to (20), aimed at easing its computation. Contrary to PolCapon, PolWISE does not replace $\mathbf{R}_{\mathbf{y}_{\mathrm{Pol}}}$ with $\mathbf{Y}_{\mathrm{Pol}}$, but with the block matrix

$$\mathbf{C}=\begin{bmatrix}\mathbf{R}_{\mathbf{y}p=1} & \mathbf{0} & \mathbf{0}\\ \mathbf{0} & \mathbf{R}_{\mathbf{y}p=2} & \mathbf{0}\\ \mathbf{0} & \mathbf{0} & \mathbf{R}_{\mathbf{y}p=P}\end{bmatrix}. \tag{21}$$

Matrix $\mathbf{C}$ contains matrices $\{\mathbf{R}_{\mathbf{y}p}\}_{p=1}^{P}$ at its main diagonal, modeled each as in (4). The usage of matrix $\mathbf{C}$ to approximate $\mathbf{R}_{\mathbf{y}_{\mathrm{Pol}}}$ infers dependency on vectors $\{\mathbf{b}_{p}\}_{p=1}^{P}$, i.e., the PSP of each polarization channel.

The true PSP is unknown, nonetheless, it can be estimated through focusing techniques like MSF, Capon, or MUSIC. Moreover, instead of focusing one polarization channel at a time, the polarimetric versions of such techniques [7] recover the contributions of each polarization channel at once. Utilizing PolCapon, by instance, yields

$$\left\{\mathbf{e}_{m}=\left\{\hat{b}_{\mathrm{PolCapon}_{m}p}\right\}_{p=1}^{P}=w_{m_{\min}}^{-1}\left\{v_{m_{\min}p}\right\}_{p=1}^{P}\right\}_{m=1}^{M}, \tag{22}$$

with $w_{m_{\min}}$ and $\mathbf{v}_{m_{\min}}$ retrieved from (16).

PolWISE recognizes that $1/\mathbf{u}_{m}^{+}\mathbf{R}_{\mathbf{y}_{\mathrm{Pol}}}^{-1}\mathbf{u}_{m}$ in (17) is actually the polarimetric PSP vector $\mathbf{b}_{\mathrm{Pol}}$ [see (14)]. Yet, the true polarimetric PSP is not known and requires to be estimated. In this order of ideas, vectors $\{\mathbf{e}_{m}\}_{m=1}^{M}$ in (22) are utilized as input and to estimate matrix $\mathbf{C}$ in (21). Consequently, (20) can be reduced to

$$\left\{w_{m_{p}}\right\}_{p=1}^{P},\quad\left\{\mathbf{v}_{m_{p}}\right\}_{p=1}^{P}$$

$$=\mathrm{eigen}\left\{\left(\mathbf{B}_{m}^{+}\hat{\mathbf{C}}^{-1}\mathbf{Y}_{\mathrm{Pol}}\hat{\mathbf{C}}^{-1}\mathbf{B}_{m}\right)\odot\mathbf{E}_{m}\right\}, \tag{23}$$

with matrix $\mathbf{E}_{m}=[\mathbf{e}_{m}^{\mathrm{T}},\,\ldots,\,\mathbf{e}_{m}^{\mathrm{T}}]$ of size $P\times P$.

Vector $\mathbf{e}_{m}$ can be retrieved by means of different polarimetric focusing techniques (e.g., PolMSF, PolCapon, or PolMUSIC [7]); thus, seeking to converge into a unique solution, PolWISE

is introduced as an iterative procedure via

$$\left\{\left\{\hat{b}_{\mathrm{PolWISE}_{m}p}^{[i+1]}\right\}_{p=1}^{P}=\frac{\mathrm{tr}\left\{\mathbf{Y}_{\mathrm{Pol}}\right\}}{\mathbf{B}_{m}^{+}\mathbf{B}_{m}}\,w_{m_{\max}}^{[i]}\left\{v_{m_{\max}p}^{[i]}\right\}_{p=1}^{P}\right\}_{m=1}^{M},$$

$$i=0,\,\ldots,\,I; \tag{24}$$

with $w_{m_{\max}}$ and $\mathbf{v}_{m_{\max}}$ as in (23),

$$\left\{\mathbf{e}_{m}^{[i+1]}=\left\{\hat{b}_{\mathrm{PolWISE}_{m}p}^{[i+1]}\right\}_{p=1}^{P}\right\}_{m=1}^{M}, \tag{25}$$

and with $\{\mathbf{e}_{m}^{[i=0]}\}_{m=1}^{M}$ recovered using a conventional polarimetric focusing technique like PolCapon in (22).

A. Regularization Parameter Selection

As discussed previously, factor N_{0} in (2) plays the role of a regularization parameter, key to avoid under/over regularization. This parameter is required to build block matrix $\hat{\mathbf{C}}$, an estimate of (21). All matrices $\{\hat{\mathbf{R}}_{\mathbf{y}p}\}_{p=1}^{P}$ inside $\hat{\mathbf{C}}$ are assumed sharing a common value N_{0}.

Aimed at properly selecting such regularization parameter, previous related studies [9] recommend using the L-Curve method. Described next for the single channel case, it is simple to extend the L-Curve method to the polarimetric configuration. Given a set of candidates $\{N_{0n}\}_{n=1}^{N}$, this technique consists in forming a smooth curve (with the shape of a letter "L") by plotting a collection of points

$$L_{C}\left(N_{0n}\right)=\left[\ln\left\{\|\mathbf{A}\hat{\mathbf{s}}\left(N_{0n}\right)-\mathbf{y}\|\right\},\ln\left\{\|\hat{\mathbf{s}}\left(N_{0n}\right)\|\right\}\right] \tag{26}$$

with $\{\hat{\mathbf{s}}\left(N_{0n}\right)=\mathbf{F}(N_{0n})\mathbf{y}\}_{n=1}^{N}$. The proper value for N_{0} corresponds to the point at the corner of the L-curve.

Note that expression (26) requires a solution operator $\mathbf{F}$ to estimate the complex reflectivity vector $\mathbf{s}$. At the same time, this operator must be utilized to recover the PSP, such that $\hat{\mathbf{b}}=\{\mathbf{F}\mathbf{y}\mathbf{y}^{+}\mathbf{F}^{+}\}_{\mathrm{diag}}=\{\mathbf{F}\mathbf{Y}\mathbf{F}^{+}\}_{\mathrm{diag}}$. For example, Tikhonov's regularization employs $\mathbf{F}=(\mathbf{A}^{+}\mathbf{A}+N_{0}\mathbf{I})\mathbf{A}^{+}$ [8]. The approach described previously infers two main disadvantages. On one hand, the scattering vector $\mathbf{y}$ needs to be provided; on the other hand, the employed solver (e.g., WISE) must be represented with a solution operator $\mathbf{F}$. These two conditions might not be always satisfied.

In order to avoid these issues, (26) is modified to work exclusively with data covariance matrices

$$L_{C}\left(N_{0n}\right)$$

$$=\left[\ln\left\{\|\left\{\hat{\mathbf{R}}_{\mathbf{y}}\right\}_{\mathrm{diag}}-\left\{\mathbf{Y}\right\}_{\mathrm{diag}}\|\right\},\ln\left\{\|\hat{\mathbf{b}}\left(N_{0n}\right)\|\right\}\right]. \tag{27}$$

The polarimetric version of (27) replaces matrix $\mathbf{Y}$ with $\mathbf{Y}_{\mathrm{Pol}}$ and matrix $\hat{\mathbf{R}}_{\mathbf{y}}$ with matrix $\hat{\mathbf{C}}$.

We refer to the algorithm in [10] to find the corner of the L-curve. Using the Menger's curvature of a circumcircle, local curvatures within the L-curve are computed using three sampled points. The value assigned to N_{0} corresponds to the maximum positive curvature of the L-curve. Being a maximization problem, a search method (e.g., golden section) is utilized to select N_{0} more efficiently.

Although the L-Curve method offers satisfactory approximations, the setting of N_0 is not considered optimal. In fact, there is no known technique for the optimal selection of regularization parameters [21]. Furthermore, factor N_0 should be selected ideally at each iteration; however, this is unpractical for real scenarios, because of the high computational complexity. Therefore, factor N_0 is chosen only once, before the PolWISE iterative procedure starts.

B. Stopping Rule

The PolWISE iterative procedure aims to converge into a unique solution, overcoming the usage of different methods to compute a first estimate of the PSP. Moreover, this strategy also aids easing inaccuracies in the regularization parameter N_0. Yet, wrong number of iterations may result in under/over regularization. Perturbation errors (i.e., $\mathbf{y} + \Delta\mathbf{y}$, $\mathbf{Y} + \Delta\mathbf{Y}$) might not be appropriately suppressed or/and errors due to regularization might be introduced

Taking the latter into account, a stopping rule is employed to detect convergence, avoiding unnecessary iterations. Correspondingly, the PolWISE iterative procedure terminates after reaching a solution that maximizes the KL information function [11], [13, Appendix C]

$$\int p\left(\mathbf{y}\right) \ln\left\{\frac{p\left(\mathbf{y}\right)}{\hat{p}\left(\mathbf{y}\right)}\right\} d\mathbf{y}, \tag{28}$$

which measures the discrepancy between the true probability density function (pdf) $p(\mathbf{y})$ and the pdf of the data model $\hat{p}(\mathbf{y})$.

The maximum likelihood (ML) solution to the TomoSAR problem is given via [8], [9]

$$\hat{\mathbf{b}}_{\mathrm{ML}} = \underset{\mathbf{b}}{\operatorname{argmin}}\left\{\ln\left\{p\left(\mathbf{y}\,|\mathbf{b}\right)\right\}\right\}, \tag{29}$$

with the log-likelihood function

$$\ln\left\{p\left(\mathbf{y}\,|\mathbf{b}\right)\right\} = \ln\left\{\det\left\{\mathbf{R_y}\right\}\right\} + \mathbf{y}^+\mathbf{R_y}^{-1}\mathbf{y}. \tag{30}$$

Using the property $\mathbf{y}^+\mathbf{R_y}^{-1}\mathbf{y} = \operatorname{tr}\left\{\mathbf{R_y}^{-1}\mathbf{y}\mathbf{y}^+\right\} = \operatorname{tr}\{\mathbf{R_y}^{-1}\mathbf{Y}\}$, the usage of the scattering vector $\mathbf{y}$ is avoided, such that

$$\ln\left\{p\left(\mathbf{y}\,|\mathbf{b}\right)\right\} = \ln\left\{\det\left\{\mathbf{R_y}\right\}\right\} + \operatorname{tr}\left\{\mathbf{R_y}^{-1}\mathbf{Y}\right\}. \tag{31}$$

Note that the true correlation matrix $\mathbf{R_y}$ is unknown and must be estimated. Finally, the polarimetric version of (31) replaces matrix $\mathbf{Y}$ with $\mathbf{Y}_{\mathrm{Pol}}$ and matrix $\hat{\mathbf{R}}_{\mathbf{y}}$ with matrix $\hat{\mathbf{C}}$.

Making use of (31), AIC [11], [13, Appendix C] is employed to maximize the KL information function in (28) by minimizing

$$\mathrm{AIC}\left(\hat{\mathbf{b}}^{[i]}\right) = -\ln\left\{p\left(\mathbf{y}\,\middle|\hat{\mathbf{b}}^{[i]}\right)\right\} + i,$$

$$i = 1,\,\dots,\,I\,. \tag{32}$$

In a similar manner, BIC [11], [13, Appendix C] is defined as the minimizer of

$$\mathrm{BIC}\left(\hat{\mathbf{b}}^{[i]}\right) = -\ln\left\{p\left(\mathbf{y}\,\middle|\hat{\mathbf{b}}^{[i]}\right)\right\} + 0.5\cdot i\cdot\ln\left\{L\right\},$$

$$i = 1,\,\dots,\,I; \tag{33}$$

whereas EDC [22] as the minimizer of

$$\mathrm{EDC}\left(\hat{\mathbf{b}}^{[i]}\right) = -\ln\left\{p\left(\mathbf{y}\,\middle|\hat{\mathbf{b}}^{[i]}\right)\right\} + i\cdot\sqrt{L\cdot\ln\left\{L\right\}},$$

$$i = 1,\,\dots,\,I; \tag{34}$$

where L is the number of flight tracks.

C. Summary

The implementation of PolWISE is summarized as follows.

Step 1: Recover $\{\mathbf{e}_m^{[i=0]}\}_{m=1}^M$ by means of a conventional polarimetric technique like PolMSF, PolCapon, or PolMUSIC. By instance, the usage of PolCapon is exemplified in (22).

Step 2: Given $\{\mathbf{e}_m^{[i=0]}\}_{m=1}^M$, a set of candidates $\{N_{0n}\}_{n=1}^N$ in (2) and the corresponding set of estimates $\{\hat{\mathbf{C}}_n\}_{n=1}^N$ in (21), select a suitable value N_0 using the polarimetric version of the L-Curve method in (27). Matrix $\mathbf{Y}_{\mathrm{Pol}}$ is constructed similar to (5), while the set $\{\hat{\mathbf{b}}(N_{0n})\}_{n=1}^N$ is calculated as in (19) with $w_{m_{\max}}$ from (23). We recommend utilizing the algorithm in [10] to find the corner of the L-curve.

Step 3: Once N_0 has been selected, perform PolWISE in (24) using the previously computed $\{\mathbf{e}_m^{[i=0]}\}_{m=1}^M$ as first input.

Step 4: Compute AIC in (32), BIC in (33), or EDC in (34) after each PolWISE iteration. Terminate the iterative procedure when the obtained values increase steadily. The minimum obtained value indicates the most appropriate PolWISE estimate $\{\hat{\mathbf{b}}_{\mathrm{PolWISE}_p}\}_{p=1}^P$ in (24). We recommend setting a maximum number of iterations.

VI. SIMULATIONS

This section assesses the capabilities of PolWISE for the single, dual and full channel cases via simulations. Sample covariance matrices $\{\mathbf{Y}_{\mathrm{Pol}}\}_{m=1}^M$ are constructed using $J = 300$ independent realizations. They gather the echoes from the scatterers displaced along the PLOS height direction. The simulated scenes comprise different number of targets, each target gathers 100 scatterers with equal reflectivity, following a Gaussian distribution. In this way, statistical uncertainty is introduced with each independent realization and we do not rely on additive noise to introduce decorrelation. Moreover, the location of the phase-centers corresponds to the mean values.

PolWISE requires a first estimate of the polarimetric PSP as zero iteration. Thus, we refer to PolCapon in (22) for such a purpose. The results presented down below (see Figs. 2–8) include the retrievals from PolCapon, PolMUSIC [7], and PolWISE (as an enhancement of PolCapon). PolMUSIC is computed utilizing a MO equal to the number of targets; whereas, PolWISE is computed using BIC as stopping rule. The quality of attained results is quantified with two metrics as follows.

1) *Root mean square error (RMSE):* When all phase-centers are detected, the RMSE between the true locations $\{\dot{z}_h\}_{h=1}^H$ and the ones found $\{\hat{\dot{z}}_h\}_{h=1}^H$ is calculated via

$$\mathrm{RMSE}\left(\dot{\mathbf{z}},\,\hat{\dot{\mathbf{z}}}\right) = \sqrt{\sum_{h=1}^H \frac{\left(\dot{z}_h - \hat{\dot{z}}_h\right)^2}{H}}. \tag{35}$$

Channel	Phase-Centers PLOS Location [m]	Spread [m]
1	$\dot{z}_1 = -3.5$, $\dot{z}_2 = -2$, $\dot{z}_3 = 5.5$ and $\dot{z}_4 = 11$	0.01
2	$\dot{z}_4 = 0$, $\dot{z}_5 = 2.6$ and $\dot{z}_6 = 11.50$	1
3	$\dot{z}_4 = 7$, $\dot{z}_5 = 16$ and $\dot{z}_6 = 17.3$	0.01

Phase-centers are recovered from the local maxima along the normalized (0 to 1) estimated pseudopower.

2) *Detection rate (DR):* Given as a percentage, represents the number of times that all phase centers are detected. Those trials with a RMSE larger than 1.5 m are ignored.

We consider a L-band SAR sensor (0.23 m wavelength) at a nominal altitude of 3000 m. The TomoSAR geometry accounts for 15 evenly distributed flight tracks, spanning a tomographic aperture of 120 m. The slant range distance from the targets to the master track is about 5000 m, with a Fourier resolution ρ_{PLOS} of approximately 4.8 m. The height range of interest Z_{PLOS} (see Fig. 1) is discretized with steps $\Delta z = \rho_{PLOS}/\varsigma$, where ς is an oversampling factor greater than or equal to one. For $\varsigma = 50$, we make use of $M = 290$ samples within a Z_{PLOS} from -7 m to 21 m.

Table I summarizes the case of study; it includes the number of simulated targets and the PLOS location of their phase-centers. Spread refers to the standard deviation of the considered Gaussian distributions.

A. Single Channel (Channel 1)

For a signal-to-noise ratio (SNR) of 10 dB and 500 Monte Carlo trials, PolMUSIC attains an average RMSE of 0.08 m and a DR of 100%; whereas, PolWISE achieves an average RMSE of 0.62 m and a DR of 97%. Conversely, PolCapon is not able of discriminating all phase-centers; therefore, its RMSE and DR cannot be computed. Fig. 2 shows a single trial out of the 500, for PolCapon, PolMUSIC, and PolWISE.

B. Dual Channel (Channels 1 and 3)

For a SNR of 15 dB and 500 Monte Carlo trials, PolMUSIC attains an average RMSE of 0.04 m and a DR of 100%; whereas, PolWISE achieves an average RMSE of 0.20 m and a DR of 100%. On the other hand, PolCapon is not able of discriminating all phase-centers; therefore, its RMSE and DR cannot be calculated. Figs. 3–5 show a single trial out of the 500, for PolCapon, PolMUSIC, and PolWISE, respectively.

C. Full Channel

For a SNR of 20 dB and 500 Monte Carlo trials, PolWISE achieves an average RMSE of 0.24 m and a DR of 100%.

The RMSE and DR of PolCapon and PolMUSIC cannot be calculated, as they are not able of detecting all phase-centers. Figs. 6–8 show a single trial out of the 500, for PolCapon, PolMUSIC, and PolWISE, correspondingly.

D. Different SNR

Aimed at analyzing the influence of the SNR on the RMSE and DR measurements, 500 Mote Carlo trials are performed for different SNR. For the single, dual and full channel cases (as in Table I), SNR of 0, 5, 10, 15, 20, and 25 dB are considered. PolWISE is computed using three stopping rules (i.e., AIC, BIC, and EDC) and a maximum number of iterations $I = 150$. Figs. 9–11 depict attained results.

E. Discussion

As seen in Figs. 9–11, PolCapon is not able to discriminate all targets for SNR below 20 dB in the single and dual channel cases. Moreover, PolCapon does not detect all targets for all considered SNRs in the full channel case. The latter allows showing one of the main advantages of PolWISE as postprocessing step, i.e., resolution enhancement. By instance, for SNR above 5 dB, PolWISE detects all targets in most of the trials of the single channel case, with a DR above 95%.

In general, the average RMSE decreases with the SNR, whereas the DR increases. All employed stopping rules (i.e., AIC, BIC, and EDC) detect convergence of the PolWISE iterative procedure successfully. The trend of the curves is independent of the stopping rule. It is important to remark that the number of iterations to achieve convergence increases with the number of channels. By instance, for a SNR of 15 dB, PolWISE requires of about 30 iterations for single channel, whereas dual and full channel entail approximately 70 and 100 iterations, correspondingly. Dual and full channel require of more iterations to prevent the false occurrence of backscattering sources; the more iterations, the more refined the result.

In order to attain a DR close to 100%, increasingly high SNR ratio is needed for the single, dual and full channel cases. Accordingly, PolWISE requires of SNR above 5 dB for single channel, SNR above 15 dB for dual channel and SNR above 20 dB for full channel. Note that PolWISE detects more easily point-type like targets than distributed targets. For the full channel case, which includes distributed targets, significantly more SNR is required in order to discriminate all phase-centers. For lower SNR, PolWISE treats some distributed targets as noise, suppressing them.

PolWISE does not preserve radiometric accuracy, as it only focusses on locating the positions from where most backscattering comes. Moreover, PolWISE is not capable of recovering the contour of the true PSP, i.e., how all scatterers distribute along PLOS height direction. Observe the output in Fig. 8(d); for an adequate SNR, PolWISE estimates all phase-centers (including those of the distributed targets) but not the outline of the actual PSP.

PolMUSIC performs better than PolWISE in the single channel case for SNR above 10 dB and also in the dual channel case for SNR above 5 dB. In both the single and dual channel cases, PolMUSIC attains a DR of 100% and an average RMSE below
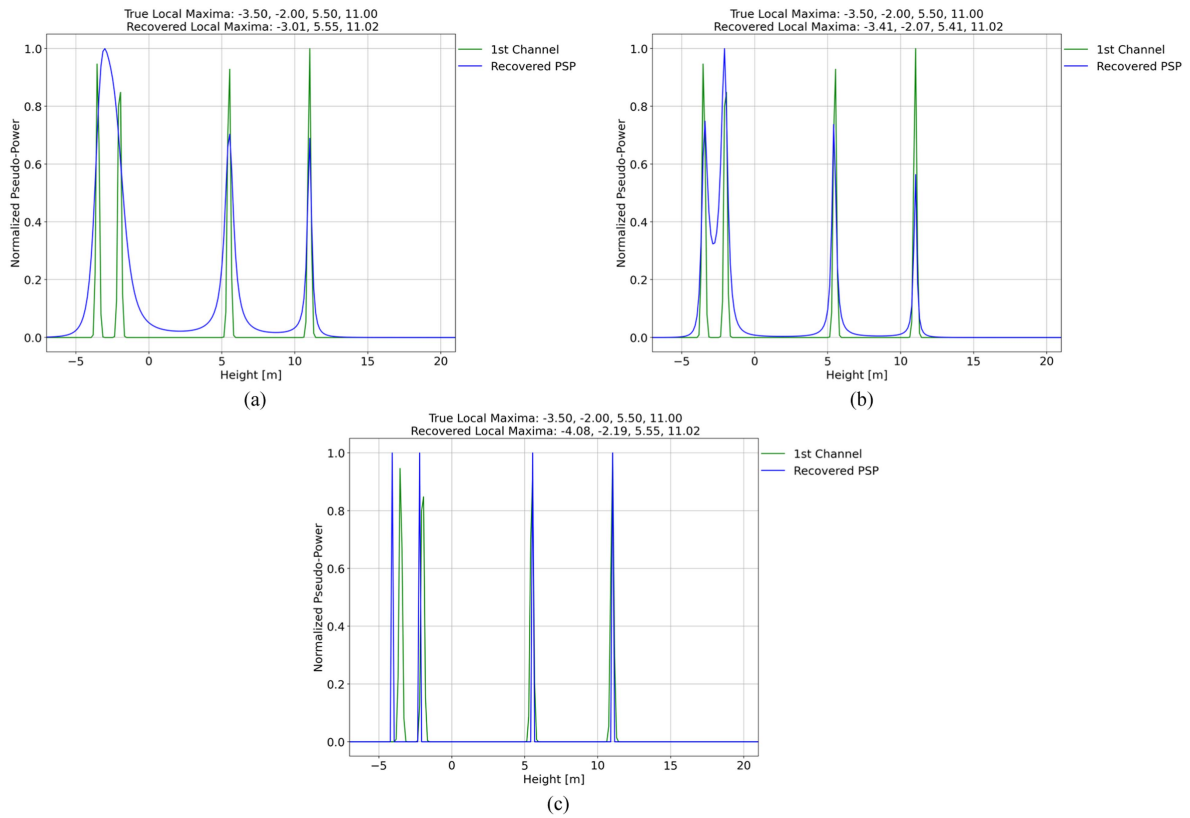
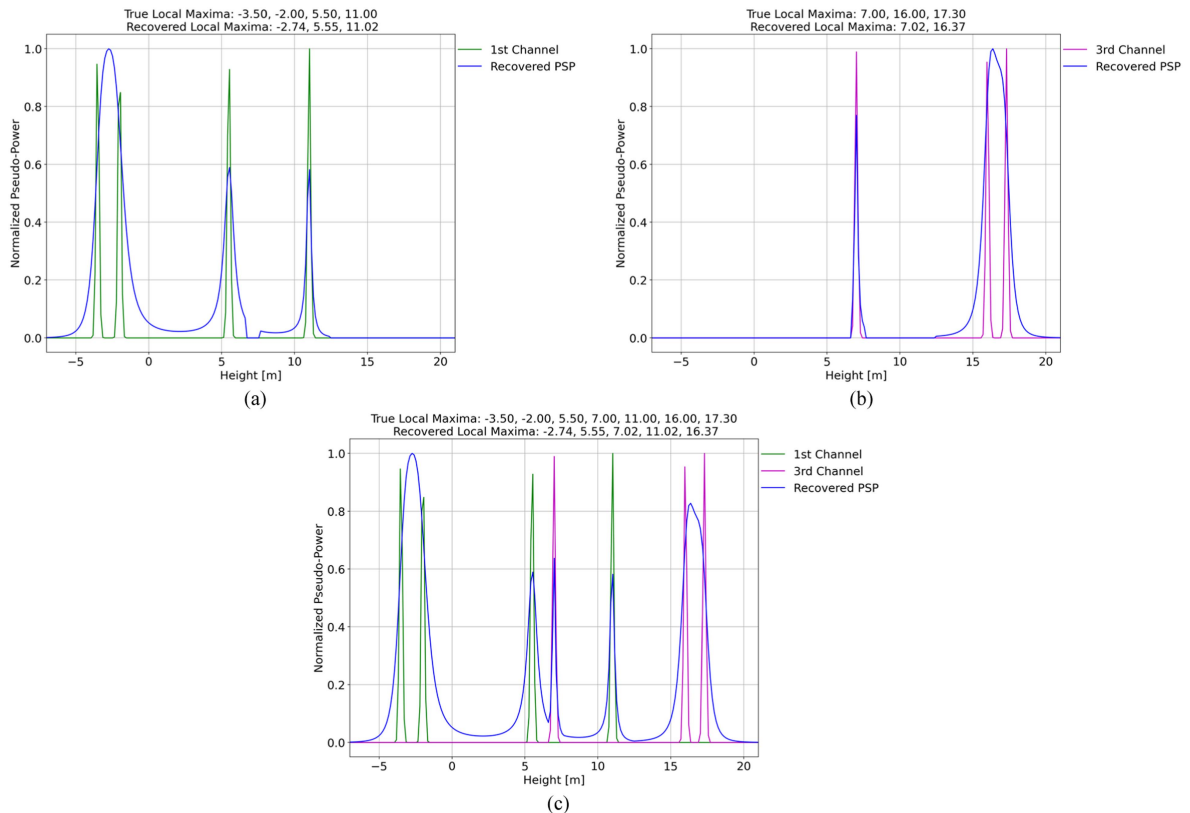Fig. 2.   Single channel. (a) PolCapon. (b) PolMUSIC. (c) PolWISE.

Fig. 3.   PolCapon dual channel. (a) First channel. (b) Third channel. (c) Combined channels.
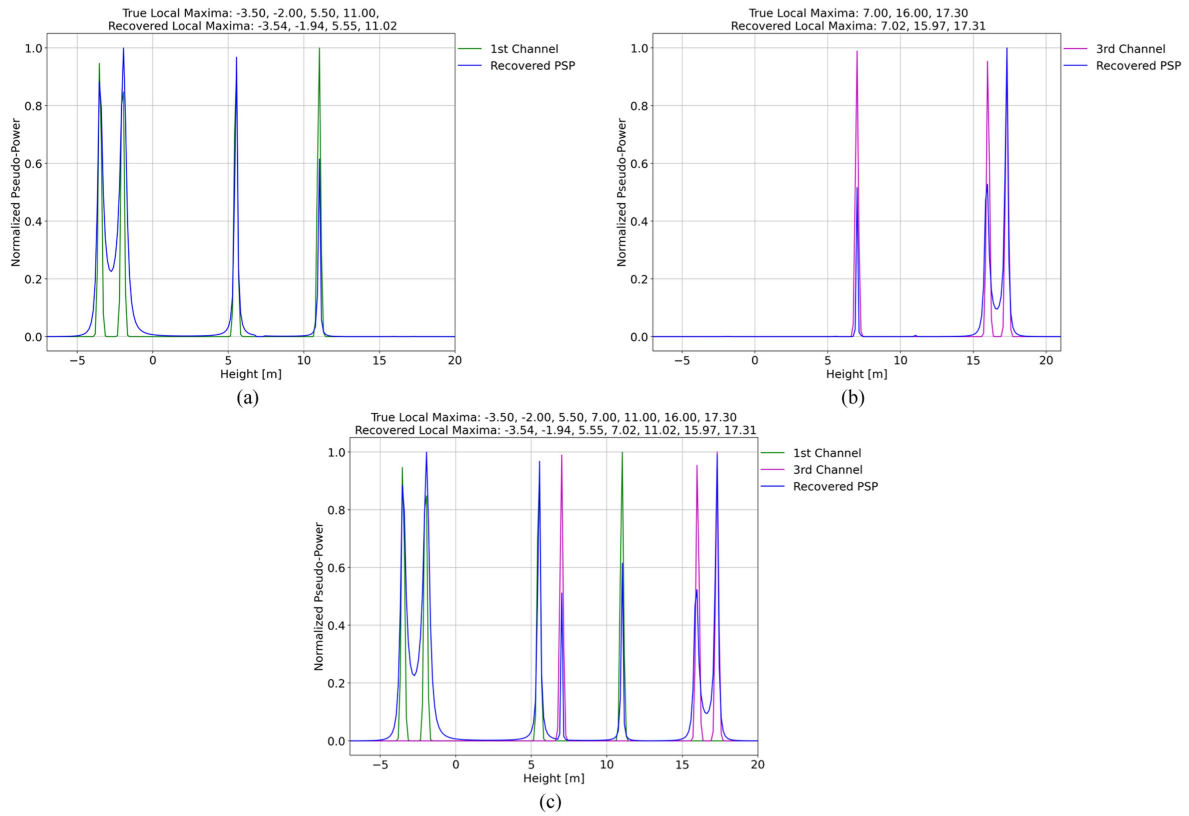
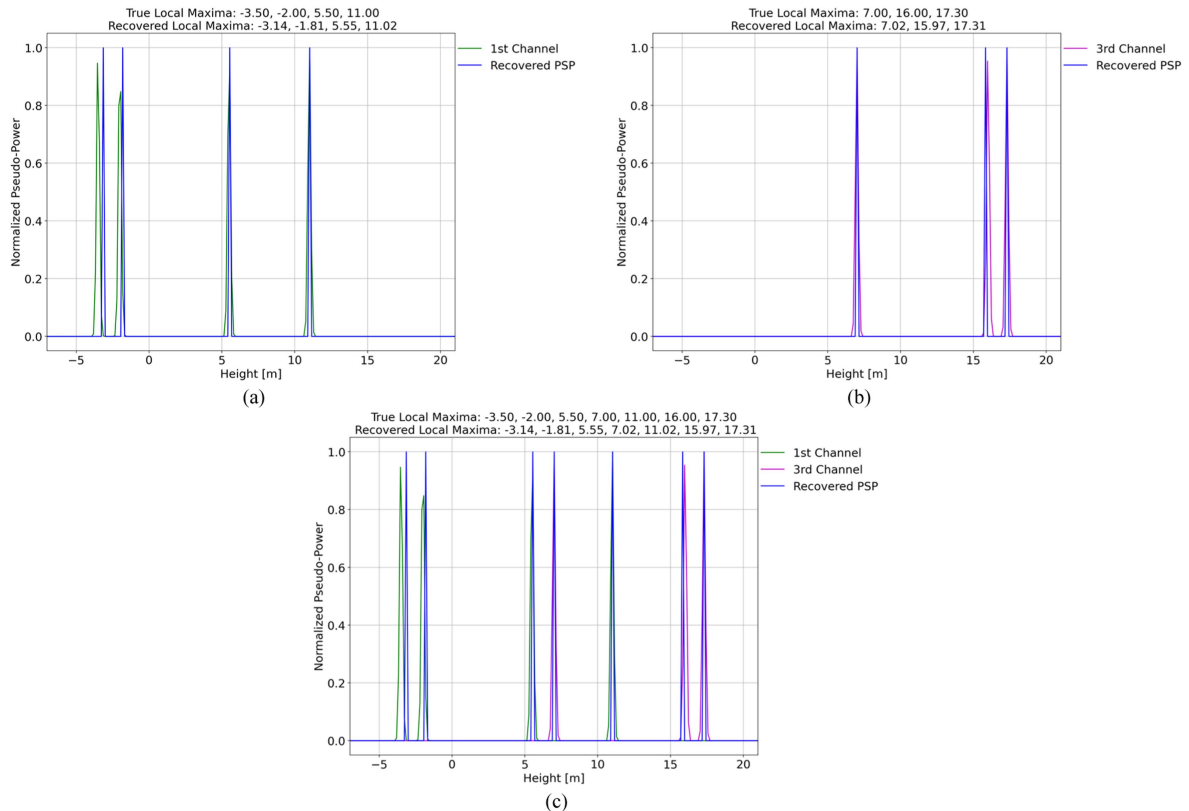Fig. 4. PolMUSIC dual channel. (a) First channel. (b) Third channel. (c) Combined channels.

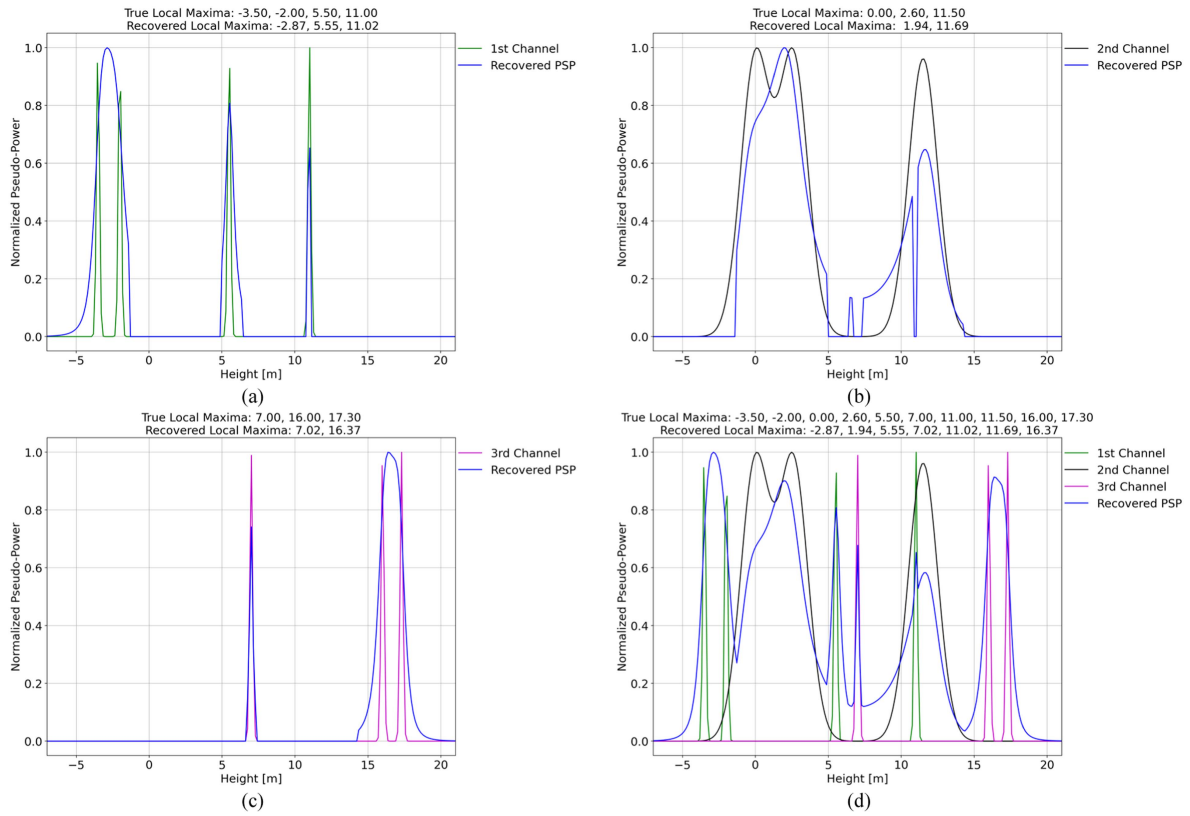Fig. 5. PolWISE dual channel. (a) First channel. (b) Third channel. (c) Combined channels.

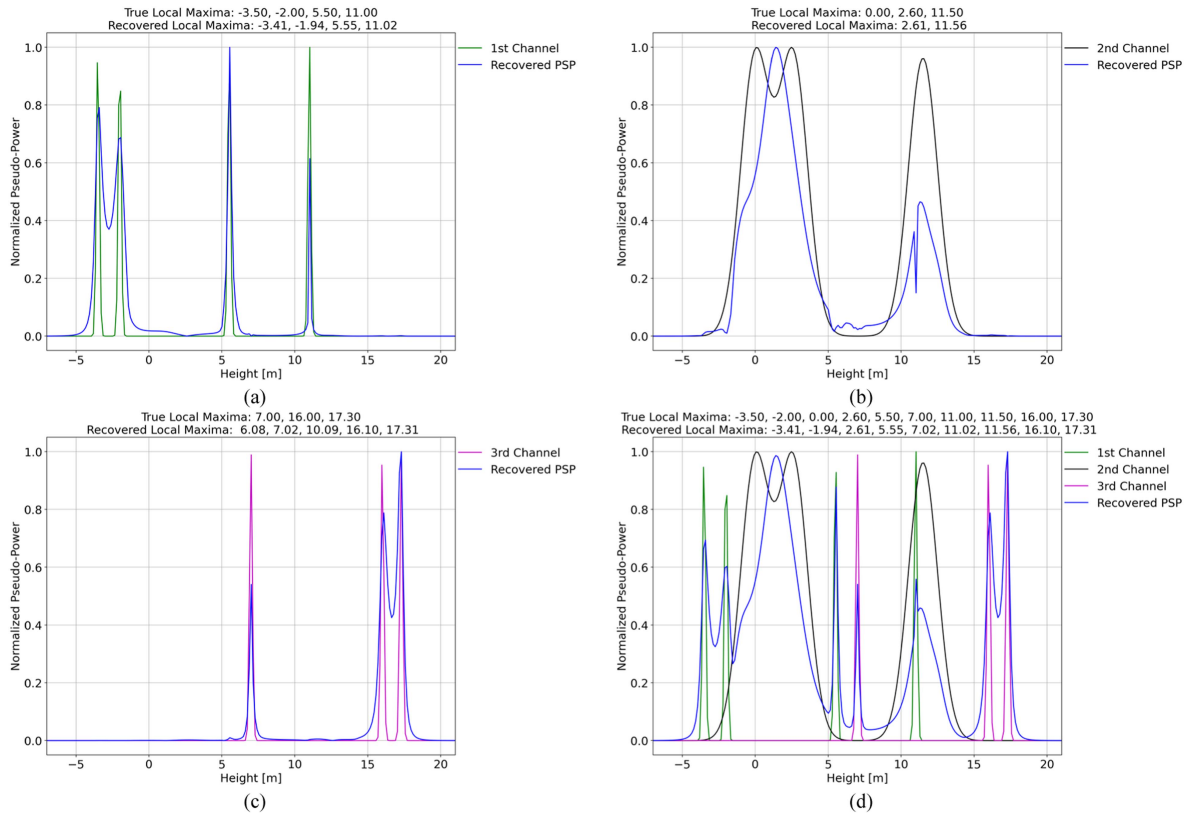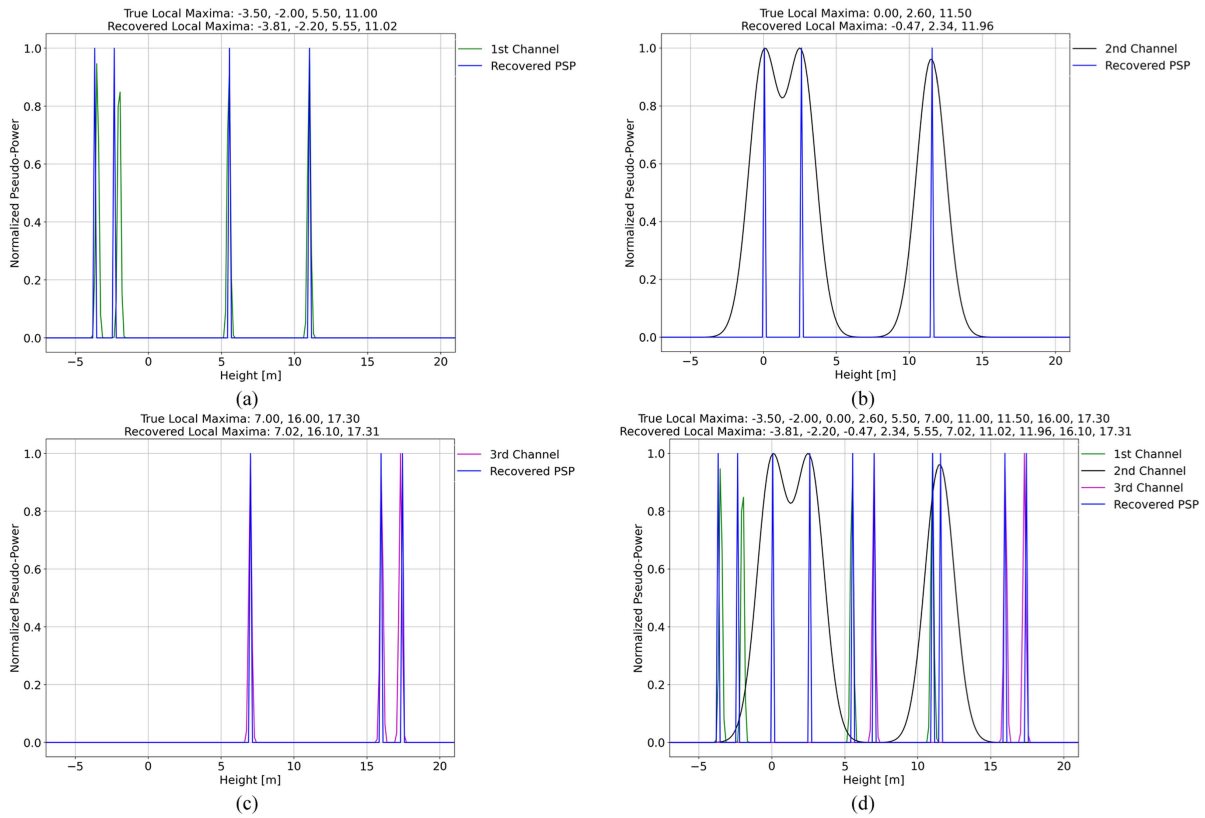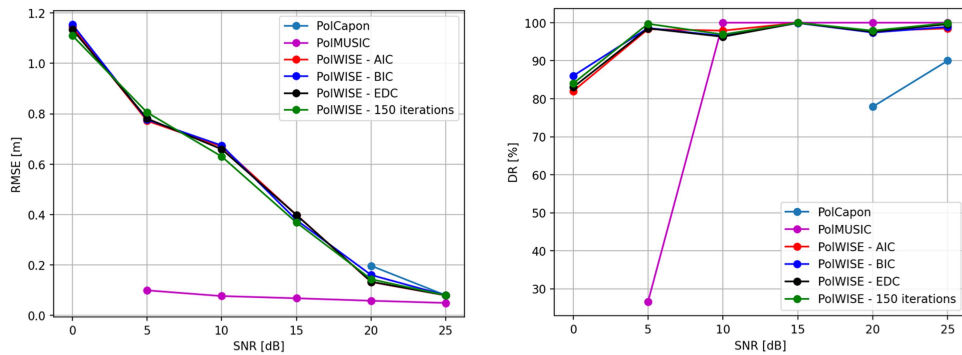Fig. 6.   PolCapon full channel. (a) First channel. (b) Second channel. (c) Third channel. (d) Combined channels.

Fig. 7.   PolMUSIC full channel. (a) First channel. (b) Second channel. (c) Third channel. (d) Combined channels.

Fig. 8. PolWISE full channel. (a) First channel. (b) Second channel. (c) Third channel. (d) Combined channels.

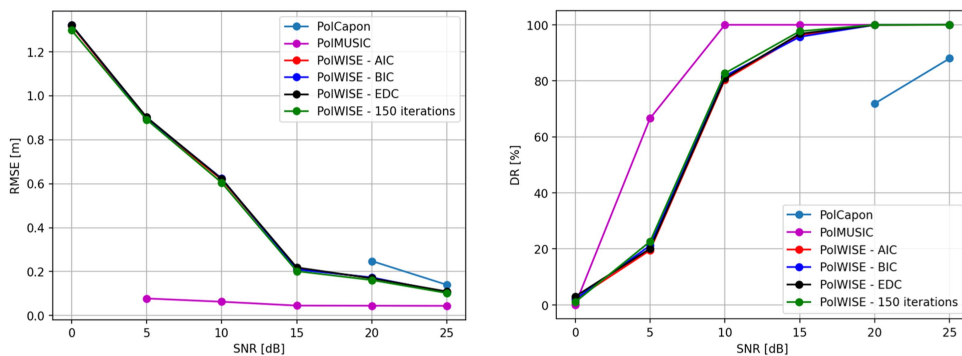Fig. 9. Single channel. (Left) Average RMSE against SNR. (Right) DR against SNR.

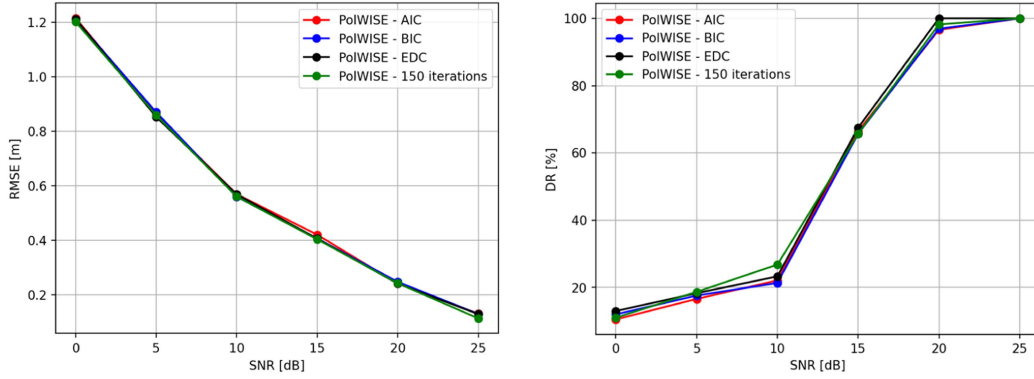Fig. 10. Dual channel. (Left) Average RMSE against SNR. (Right) DR against SNR.

Fig. 11.   Full channel. (Left) Average RMSE against SNR. (Right) DR against SNR.

0.1 m for SNR above 10 dB. Note that, for a SNR of 5 dB, PolMUSIC achieves higher DR for dual channel than for single channel. PolMUSIC seems to benefit from a higher MO in the dual channel case.

PolWISE performs better than PolMUSIC for full channel, as PolMUSIC is not able of detecting all targets for all considered SNRs. As expected, PolMUSIC functions better with point-type targets than with distributed targets.

In general, the performance of PolWISE depends on the accuracy of its first input, retrieved in this article via PolCapon. The higher RMSE attained in the single and dual channel cases (compared to PolMUSIC) is due to those pairs of targets that PolCapon detects as a single target. Specifically, those located at -3.5 m and -2 m in the first channel [see Fig. 2(a)] and those located at 16 m and 17.3 m in the third channel [see Fig. 3(b)]. In such instances, the information provided by PolCapon is not accurate enough to retrieve results like those of PolMUSIC. This aspect also impacts the DR obtained, as the information given by PolCapon may not be at all times sufficient to discriminate all targets among the different trials.

As it can be seen in Figs. 9 and 10, the results achieved by PolWISE approach those of PolMUSIC for higher SNR. Although the iterative procedure of PolWISE seeks to converge into a unique solution, the simulations indicate that an adequate SNR is also necessary to achieve that goal.

Described in [12], MUSIC improves performance with the use of dedicated MO selection tools, such as those based on information theoretic criteria. In addition, WISE might be employed as prostprocessing step to enhance MUSIC's resolution. Applying this strategy to the polarimetric case is beyond the scope of this article, whose main objective is to introduce PolWISE. Nevertheless, future work plans to use PolWISE in combination with PolMUSIC.

PolWISE has higher computational complexity than conventional methods like PolCapon and PolMUSIC. By instance, it requires the inversion of matrix $\hat{\mathbf{C}}$ in (21), whose dimensions increase with the number of channels. Furthermore, PolWISE entails the selection of factor N_0 (chosen via L-Curve method), which also involves the inversion of matrix $\hat{\mathbf{C}}$. In addition to the aforementioned, the need for more iterations to converge as the number of channels grows, increases processing time considerably.

TABLE II
TomoSAR Acquisition Geometry

Track	Flight altitude [m]
1	12500
2	12500 + 30
3	12500 + 90
4	12500 + 160
5	12500 + 240
6	12500 + 400
7	12500 + 600

VII. Experimental Results

Experiments are conducted using a fully-polarimetric To-moSAR dataset at L-band, acquired in 2015 in Munich, Germany, by jet propulsion laboratory (JPL)/national aeronautics and space administration (NASA) [23]. The uninhabited aerial vehicle SAR (UAVSAR) system of JPL/NASA was mounted on a Gulfstream G-III airplane at a nominal altitude of 12.5 km, attaining a swath of 22 km and length of 60 km. Incidence angles range from 25° to 65°, whereas the noise equivalent sigma-zero ranges from -35 dB to -53 dB across the swath [24]. For 80 MHz chirp bandwidth and a wavelength of 0.24 m, the acquired single look complex (SLC) images reach a resolution of 0.8 m in azimuth and 1.66 m in range [23]. The TomoSAR acquisition geometry considers seven passes at different flight altitudes, as depicted in Table II.

Fig. 12 shows the primary image. The imagery was completed on a heading of 193°, with a vertical Fourier resolution of approximately 6 m in far range and 2.8 m in near range. Two regions of interest (ROIs) are considered, where the Maximilianeum and the Bavarian state chancellery are located, correspondingly. Both edifices are almost parallel to the sensor trajectory.

Fig. 13 displays the intensity images of the first ROI for channels HH, HV, and VV. The red rectangles indicate where the building is placed, whereas the azimuth and range indices permit identifying its position. The red line, crossing the building, specifies the orientation, along azimuth-range axes, of the
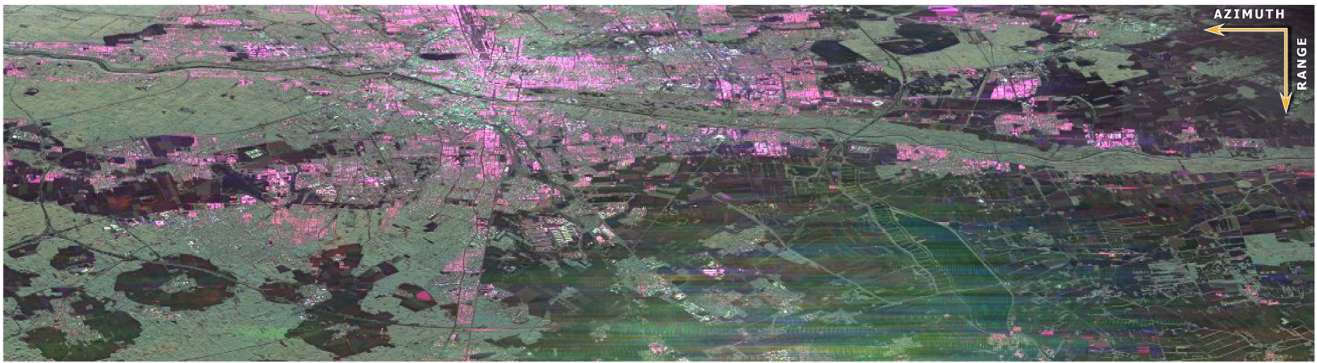
Fig. 12. SLC SAR image of the test site in Munich, Germany, 2015 (near range on top). Colors correspond to channels HH (red), VV (blue), and HV (green).
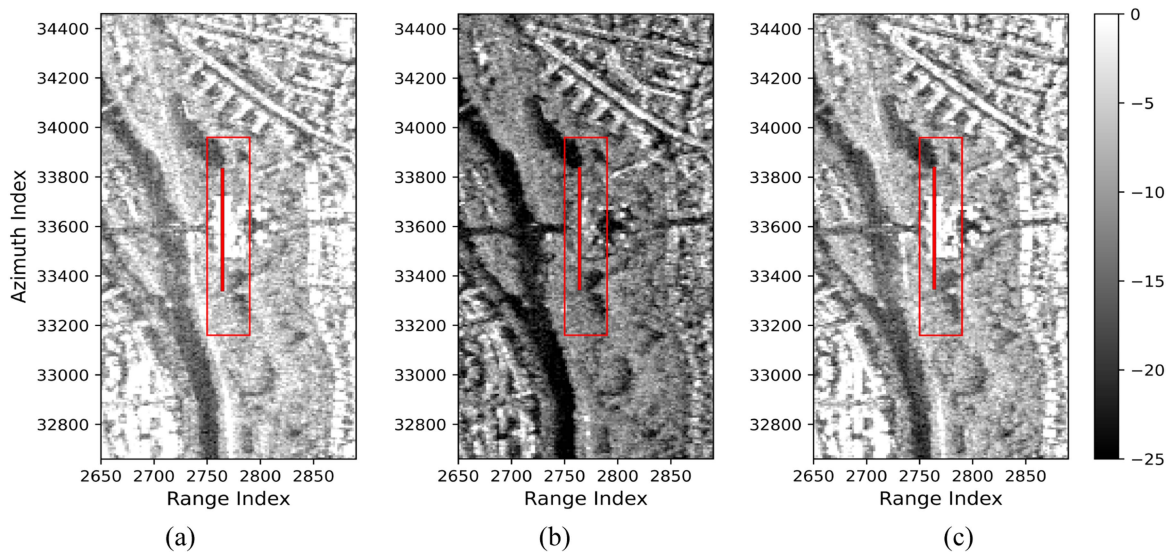

Fig. 13. Intensity images in dB from the ROI where the Maximilianeum is located. (a) HH. (b) HV. (c) VV.

tomograms presented afterward. Fig. 14 describes the test region via a Google Earth image and a polarimetric SLC SAR image. The height of the structures comprising the edifice are also specified. Figs. 15–17 show the corresponding tomograms, employing PolCapon, PolMUSIC, and PolWISE, respectively. X-axis (azimuth) is given in samples to identify easily the area from where the tomograms originate.

The MO for MUSIC is set manually to 3. BIC in (33) is utilized to terminate PolWISE. A 5×10 (range/azimuth) boxcar filter is employed to spatially average the covariance matrices. Pseudopower is presented in a dB scale, where 0 dB refers to the maximum attained value. Z_{PLOS} is discretized with steps $\Delta z = 2.8$ m / $10 = 0.28$ m. Thus, we make use of $M = 232$ samples within a Z_{PLOS} from -20 m to 45 m.

Since the addressed polarimetric focusing techniques allow retrieving the contributions from each polarimetric channel, it is possible to perform the eigenvector analysis of the corresponding 3×3 coherency matrices. Such analysis "provides a basis invariant description of the scatterer with a specific decomposition into types of scattering processes (the eigenvectors) and their relative magnitudes (the eigenvalues)"

[25]. Among the mean parameters of the dominant scattering mechanism, extracted from the coherency matrices, there is the alpha mean angle $\bar{\alpha}$. Values of $\bar{\alpha}$ close to 0° suggest single-bounce reflection, $\bar{\alpha}$ values close to 45° suggest volume reflection, and $\bar{\alpha}$ values close to 90° suggest double-bounce reflection.

Fig. 18 shows the scattering patterns retrieved from the $\bar{\alpha}$ of the dominant reflector [25, Chapter 7] for PolCapon, Pol-MUSIC, and PolWISE. A mask based on a threshold of the pseudopower is applied to set to color black those samples with low backscattering values [7]. The aim of such analysis is to show that further studies can be performed with the retrievals of focusing techniques, which have been extended to the polarimetric configuration. Besides $\bar{\alpha}$, parameters like the entropy (H) and anisotropy (A) might be also obtained [25, Chapter 7].

A similar strategy is followed for the second ROI. Fig. 19 displays the corresponding intensity images for channels HH, HV, and VV. Fig. 20 describes the test region and specifies the height of the structures comprising the Bavarian state chancellery. Figs. 21–23 present the corresponding tomograms for
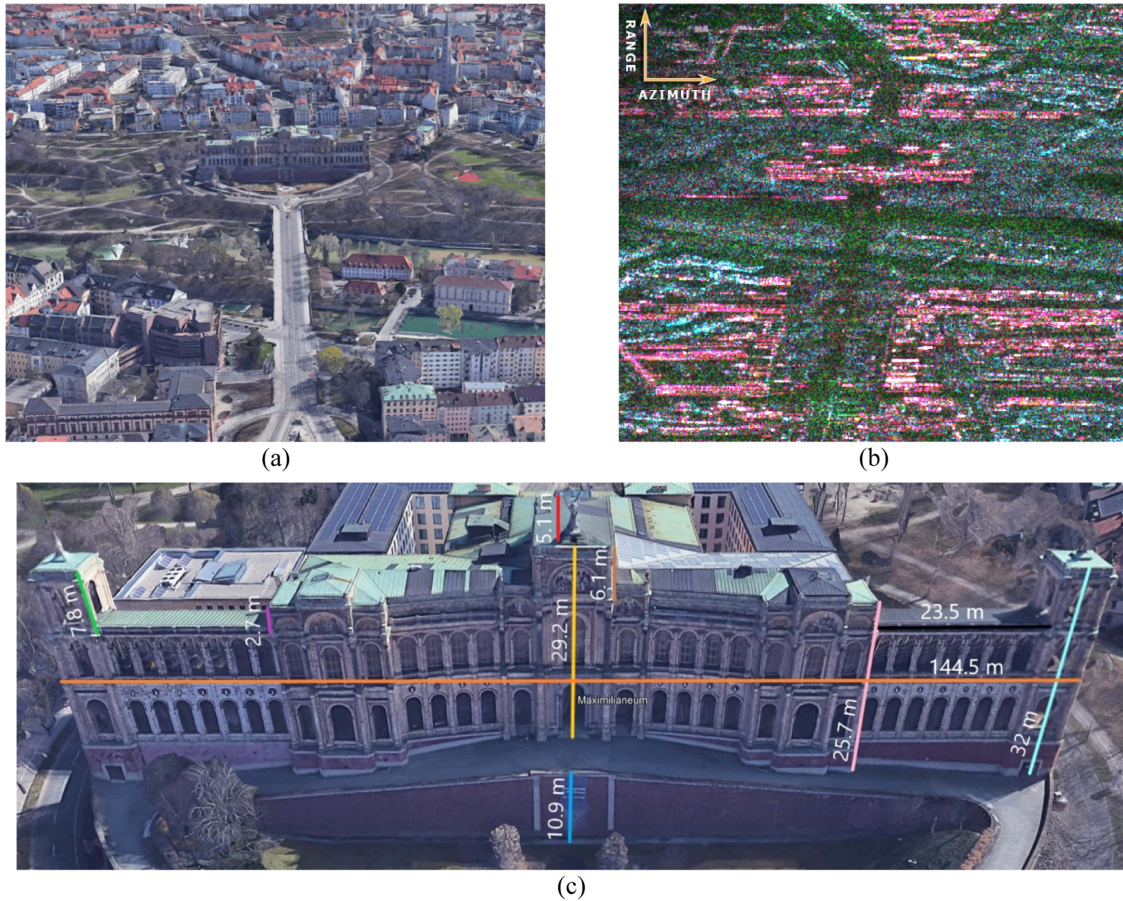
Fig. 14.   Region where the Maximilianeum is placed. (a) Google Earth image. (b) Polarimetric SLC SAR image [colors correspond to channels HH (red), VV (blue), and HV (green)]. (c) Front view of the edifice (Google Earth).

PolCapon, PolMUSIC, and PolWISE, respectively. Z_{PLOS} is discretized with steps $\Delta z = 2.8 \text{ m}/10 = 0.28 \text{ m}$. Thus, we make use of $M = 214$ samples within a Z_{PLOS} from -15 m to 45 m. Fig. 24 shows the corresponding attained $\bar{\alpha}$ values.

A. Discussion

Contrasting PolCapon, PolMUSIC and PolWISE, at first glance we can assess that PolWISE attains finer resolution, besides of performing ambiguity reduction and artefacts suppression. These enhancements facilitate estimating the height of reflectors, extracted from the local maxima along the recovered polarimetric pseudopower. The several structures comprising the edifices are easier to discern. To a limited extent, PolWISE retrieves sufficiently narrow peaks to identify numerous components at different height locations. In the case of the Maximilianeum in Fig. 17, observe the two towers at the extremes, the central building and one wing on either side. Whereas, in the case of the Bavarian state chancellery in Fig. 23, note the central building (where the dome is placed) and both wings, one on each side. The topography on the flanks of both edifices can be also observed.

PolMUSIC achieves a finer resolution than PolCapon. Moreover, it is worth recalling that the use of specific MO selection tools [12] may increase the performance of PolMUSIC. In addition, PolMUSIC can be combined with PolWISE to improve the resolution.

The polarimetric versions of Capon, MUSIC, and WISE are employed in order to separate the associated scattering mechanisms into three channels. The first channel contains mainly double bounce-reflection, the second channel volume reflection and the third channel single-bounce reflection. PolCapon and PolMUSIC provides information on certain structures in all channels, as shown in color white in Figs. 15(a), 16(a), 21(a), and 22(a). In contrast, PolWISE [see Figs. 17(a) and 23(a)] does not share information about the same structure among channels. The pseudopower profiles of each channel complement each other but do not overlap.

In line with the simulations, PolMUSIC and PolWISE perform better for point-type like targets, commonly associated to polarizations HH and VV. Note that for both edifices, Maximilianeum in Fig. 13 and Bavarian state chancellery in Fig. 19, polarization HH attains highest intensity levels; followed by VV and HV, in that order. Contrariwise, PolWISE filters out most of the contributions in HV, usually associated to distributed targets. Due to lower backscattering, some distributed targets are suppressed, since they are considered noise.

At each iteration, PolWISE pursue refining its current input and achieving super-resolution. The method concentrates first on those backscattering sources with higher energy and, sometimes, ignores (suppresses) those targets with lower backscattering.
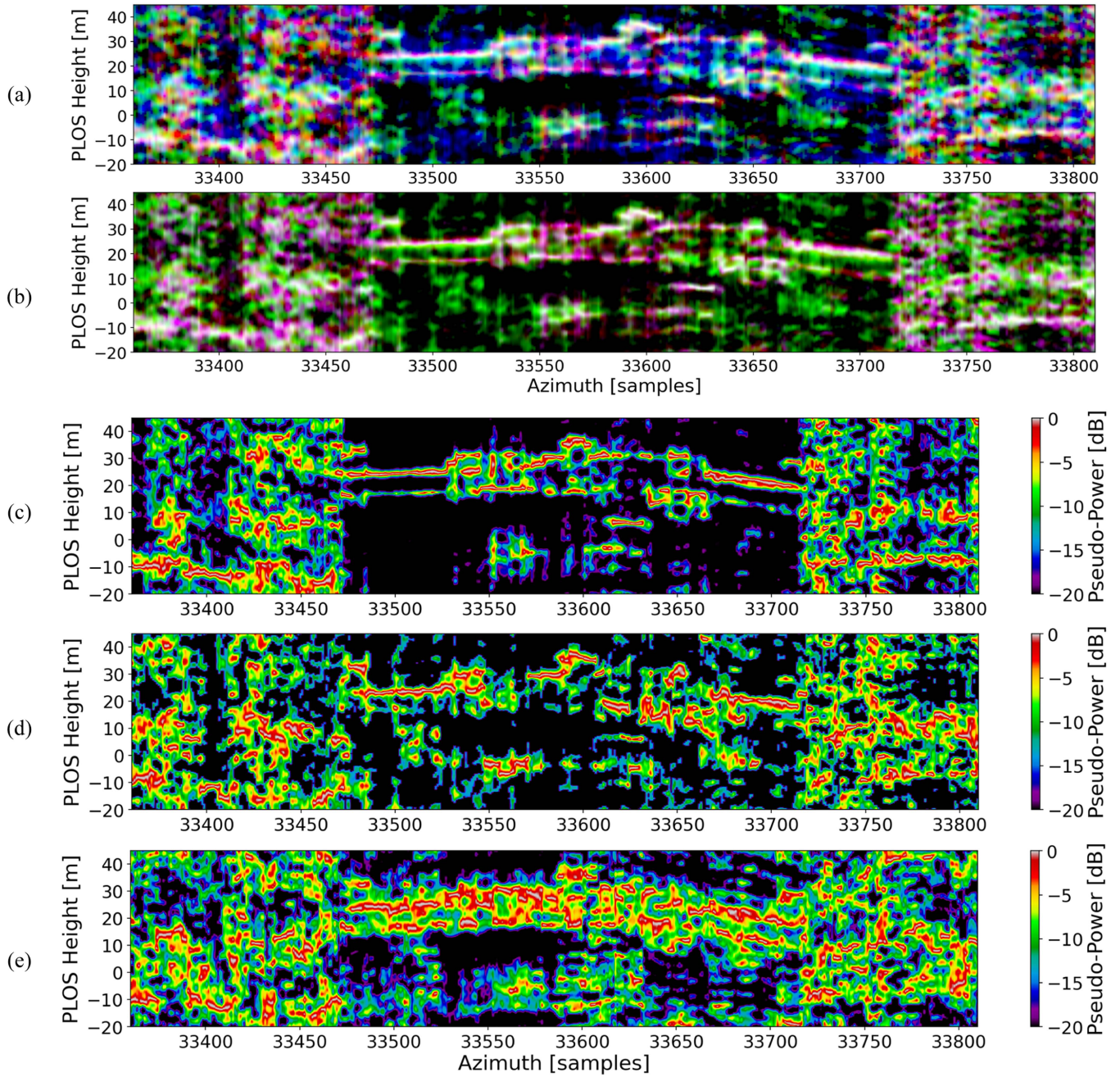
Fig. 15. PolCapon tomograms from the ROI in Fig. 13. (a) Lexicographic [Red (first Channel), Green (second Channel), Blue (third Channel)]. (b) Pauli. (c) First Channel: double-bounce reflection. (d) Second Channel: volume scattering. (e) Third Channel: single-bounce reflection.
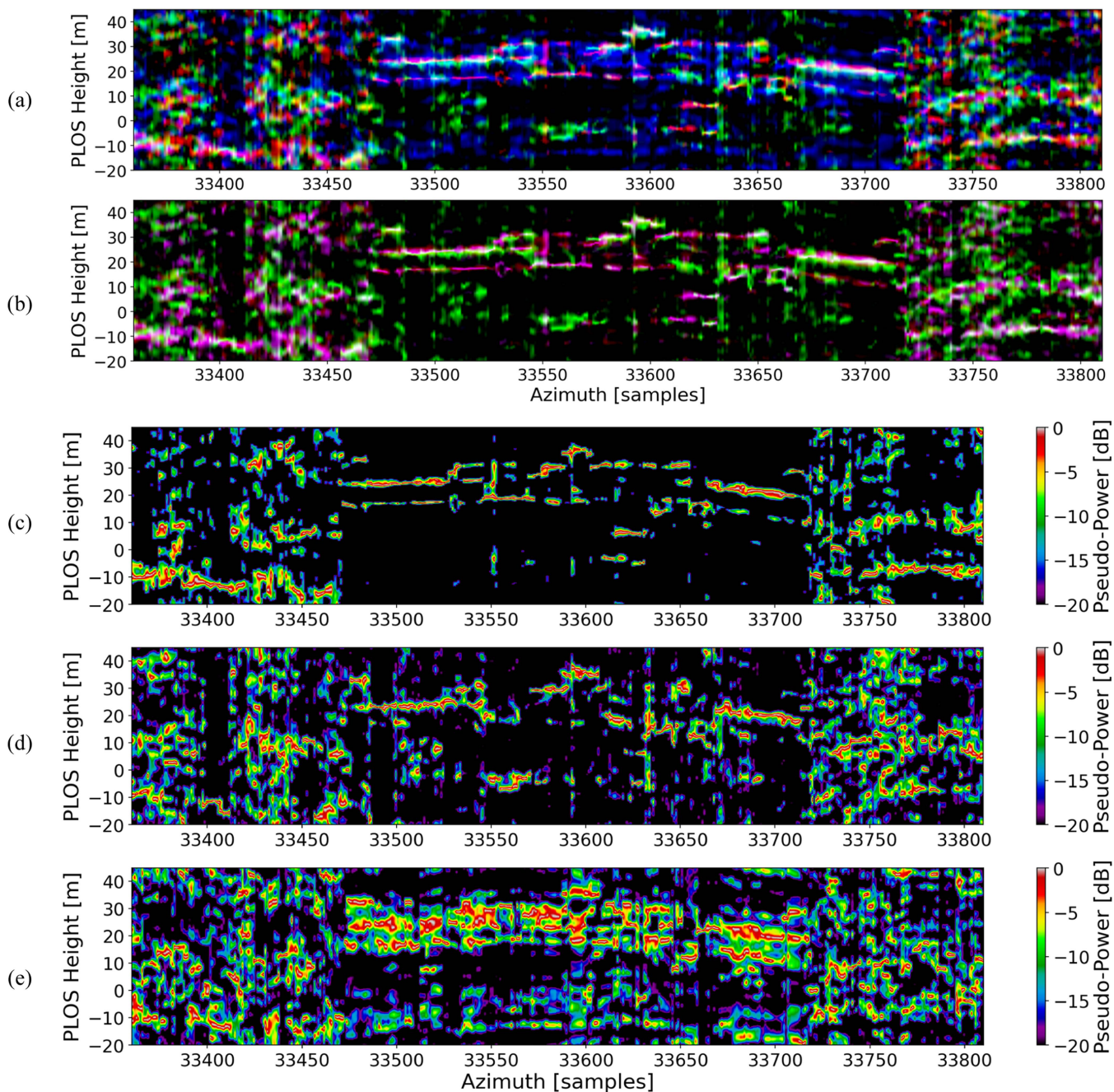
Fig. 16.   PolMUSIC tomograms from the ROI in Fig. 13. (a) Lexicographic [Red (first Channel), Green (second Channel), Blue (third Channel)]. (b) Pauli. (c) First Channel: double-bounce reflection. (d) Second Channel: volume scattering. (e) Third Channel: single-bounce reflection.
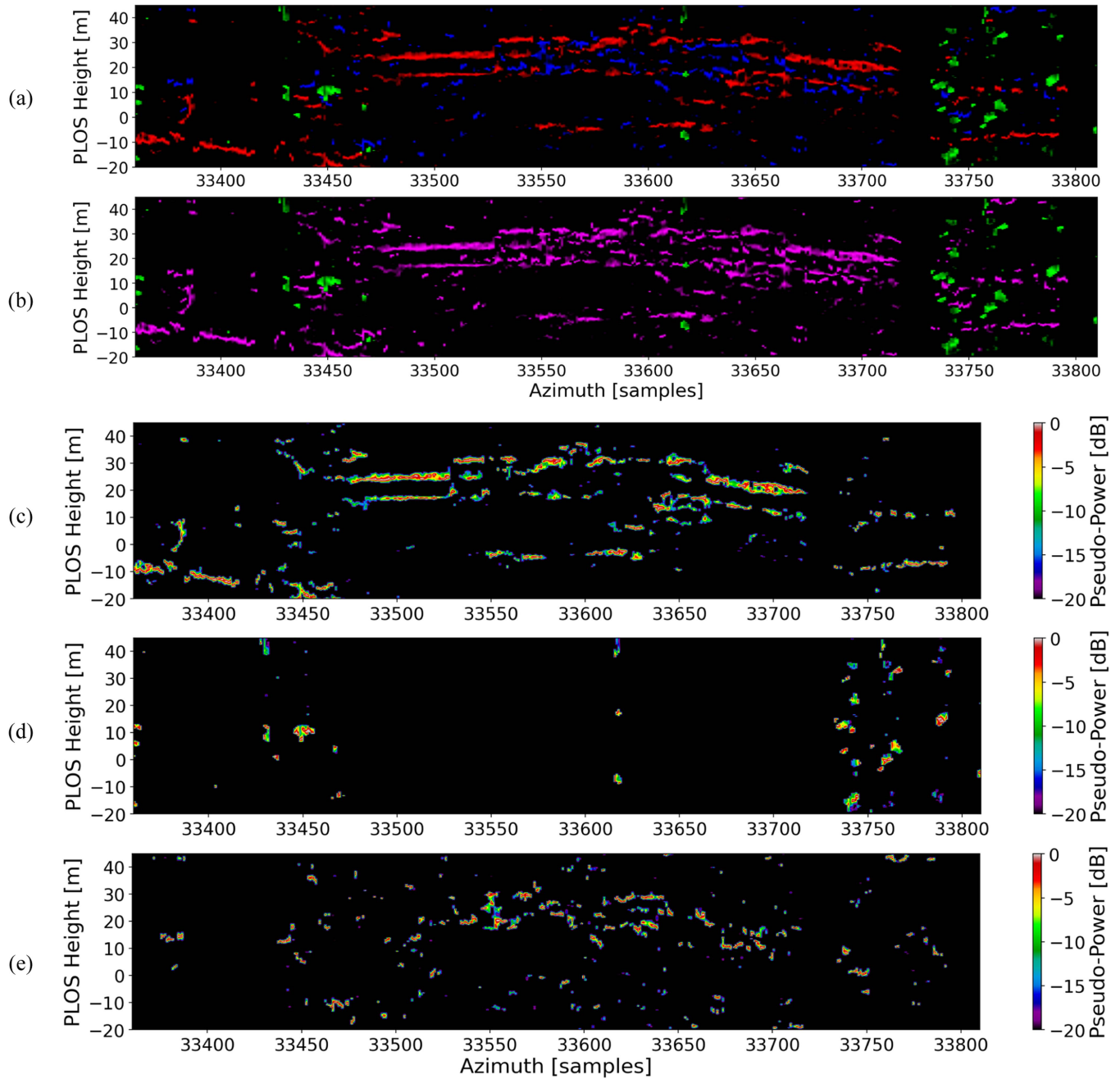
Fig. 17. PolWISE tomograms from the ROI in Fig. 13. (a) Lexicographic [Red (first Channel), Green (second Channel), Blue (third Channel)]. (b) Pauli. (c) First Channel: double-bounce reflection. (d) Second Channel: volume scattering. (e) Third Channel: single-bounce reflection.
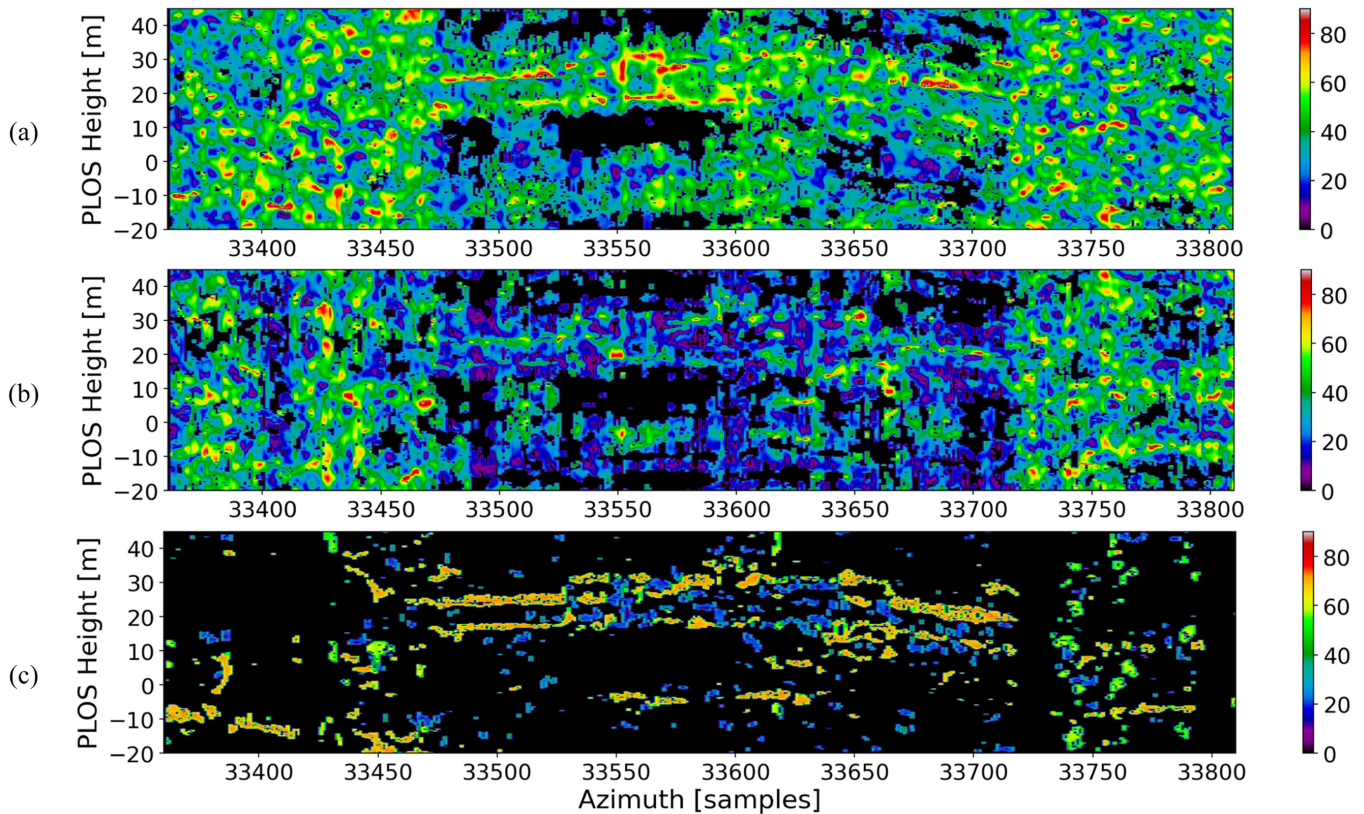
Fig. 18.   Maximilianeum: alpha mean angle $\bar{\alpha}$ in degrees. (a) PolCapon. (b) PolMUSIC. (c) PolWISE.
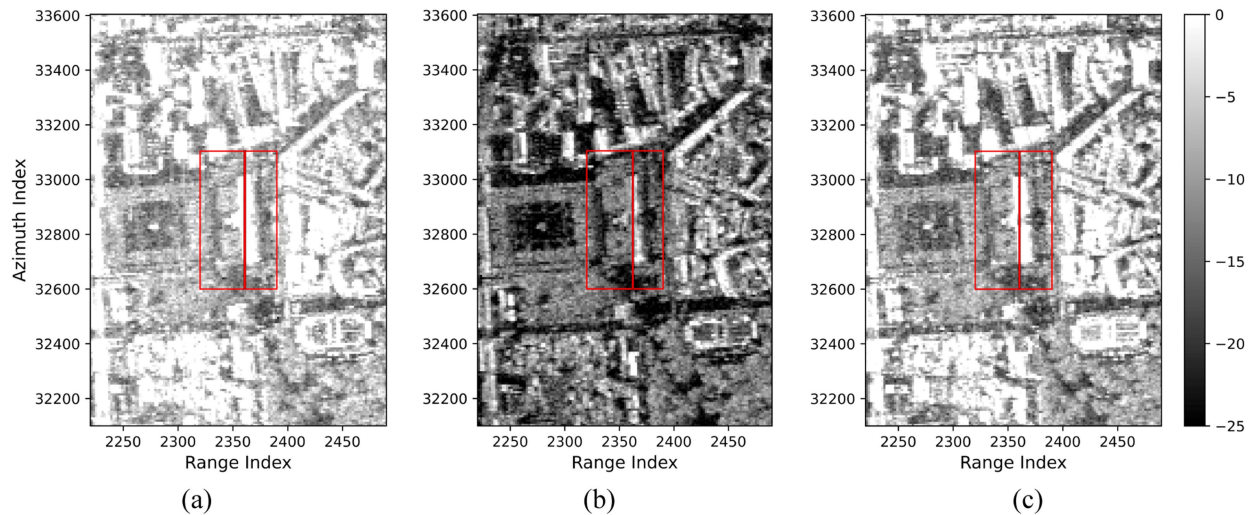

Fig. 19.   Intensity images in dB from the ROI where the Bavarian state chancellery is located. (a) HH. (b) HV. (c) VV.

Recall that a proper selection of PolWISE's regularization parameter is key to obtain good-fitted solutions. Nevertheless, due to practical reasons and to reduce computation time, such regularization parameter is chosen only once, before the iterative procedure starts. Theoretically, selecting the regularization parameter at each iteration increases the performance of PolWISE, also in the case of distributed targets; nonetheless, processing time increases meaningfully, making this approach unpractical.

In contrast to PolCapon and PolMUSIC, as seen in Figs. 18(c) and 24(c), thanks to the characteristics of PolWISE, it is easier to categorize the places where a certain type of scattering mechanism is present. In the case of the Maximilianeum, double-bounce reflection prevails at the wall-ground interaction points below the central building. Scattering at the top of the edifice and numerous targets along the walls, also correspond to double-bounce reflection. Note that the topography on the
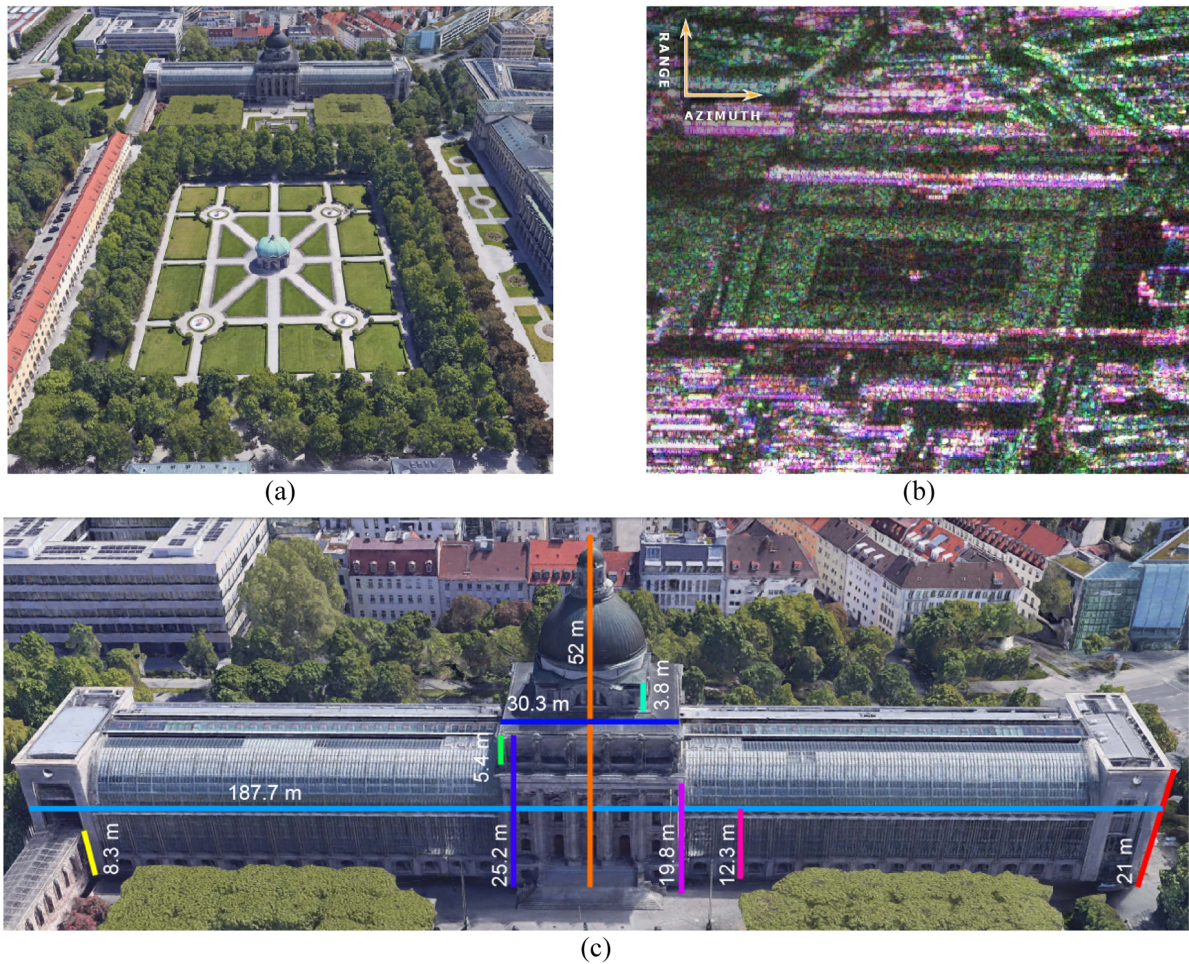
Fig. 20. Region where the Bavarian state chancellery is located. (a) Google Earth image. (b) Polarimetric SLC SAR image [colors correspond to channels HH (red), VV (blue), and HV (green)]. (c) Front view of the edifice (Google Earth).

flanks is characterized by double-bounce reflection, presumably due to tree-trunk-ground interactions. Single-bounce reflection occurs in the roof of the central building and along the walls, especially in the central building. Unlike the edifice wings, which join the central building to the towers at the extremes, the central building possesses large glazed windows, where most single-bounce reflection concentrates. Finally, volume reflection mainly occurs on the flanks of the edifice, where the vegetation is located.

In the case of the Bavarian state chancellery, backscattering from wall-ground interactions at the topographic height of about 0 m indicate double-bounce reflection. Scattering at the top of the edifice, targets at the columns and at the stairs of the central building, and targets at the dome above the central building, also correspond to double-bounce reflection. Single-bounce reflection occurs in the roof, in the dome and mainly along the glazed walls of both wings, on either side of the edifice. The topography at left hand is characterized by single-bounce reflection; whereas the topography at right hand is characterized by both, single- and double-bounce reflection. Note that most volume reflection pertains to the right flank of the edifice. This suggests double-bounce reflection due to tree-trunk-ground interactions, differing to the left flank. Finally, observe the presence of another edifice at the edge, on the right. Scattering at the top of this edifice correspond to double-bounce reflection; whereas single-bounce reflection occurs in the roof and in some targets along its walls.

Methods like PolCapon, PolMUSIC, and PolWISE increase the dimension of the observation space, aimed at calculating optimal polarization combinations [7]. Particularly, PolWISE is considered optimal in sense of WCF. Nevertheless, in order to properly solve the WCF optimization problem, PolWISE relies in the correct selection of a regularization parameter. Setting the regularization parameter wrongly, might cause misleading solutions. Furthermore, due to the nature of regularization approaches like PolWISE, some information may be filtered out after the iterative procedure is terminated. Therefore, it is recommended treating PolWISE results as information complementary to its input, in this case PolCapon.

The current research makes use of the L-Curve method [21] to select the involved regularization parameter, showing satisfactory results. Nevertheless, the L-Curve method depends on a correct range and density of sample values to perform adequately. Further research is underway to ensure proper selection of regularization parameters at all times, regardless of these factors. We are currently studying how this issue is addressed in other areas, for example in geophysical diffraction tomography [26].
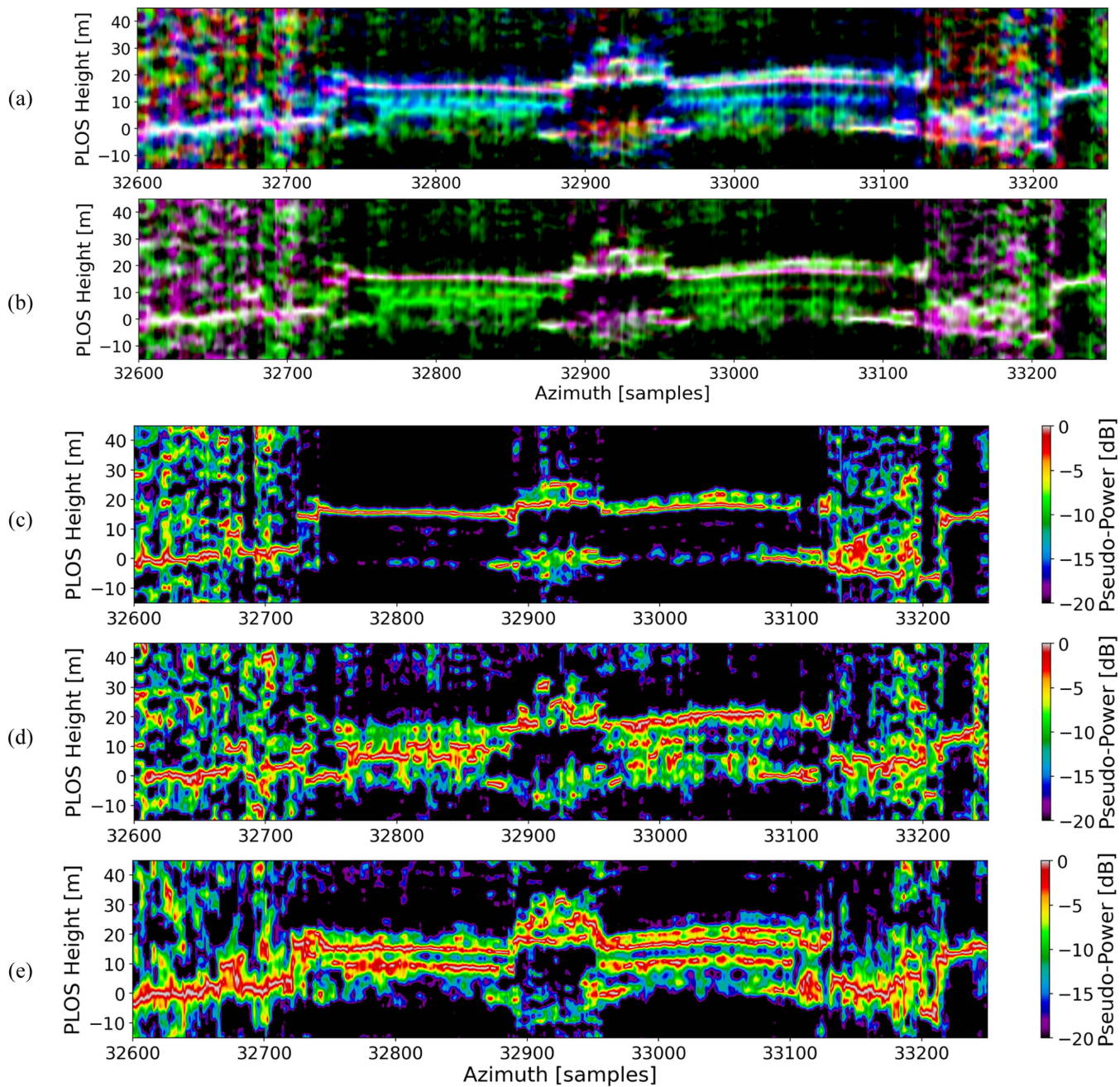
Fig. 21.   PolCapon tomograms from the ROI in Fig. 19. (a) Lexicographic [Red (first Channel), Green (second Channel), Blue (third Channel)]. (b) Pauli. (c) First Channel: double-bounce reflection. (d) Second Channel: volume scattering. (e) Third Channel: single-bounce reflection.

Fig. 22. PolMUSIC tomograms from the ROI in Fig. 19. (a) Lexicographic [Red (first Channel), Green (second Channel), Blue (third Channel)]. (b) Pauli. (c) First Channel: double-bounce reflection. (d) Second Channel: volume scattering. (e) Third Channel: single-bousnce reflection.
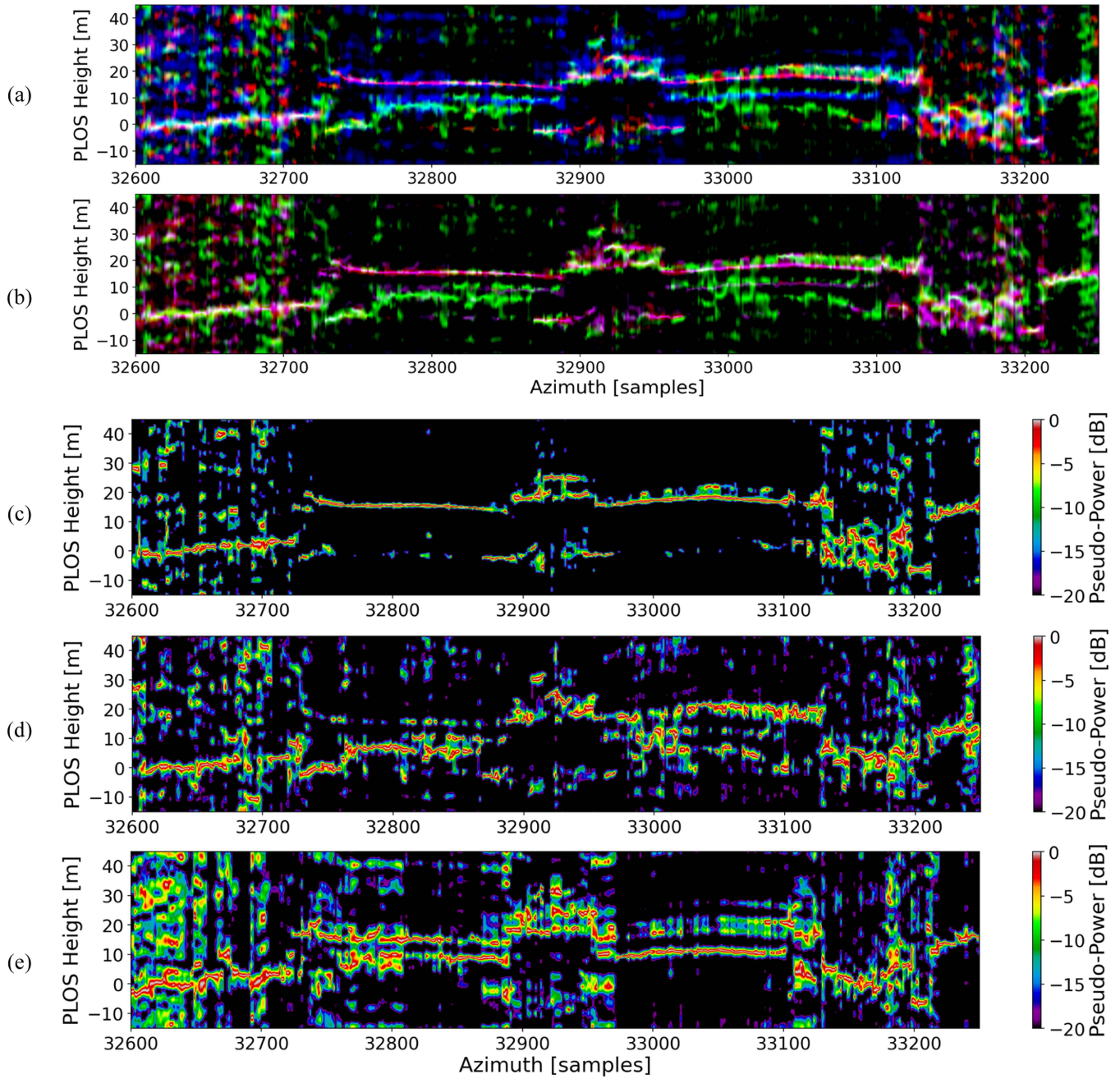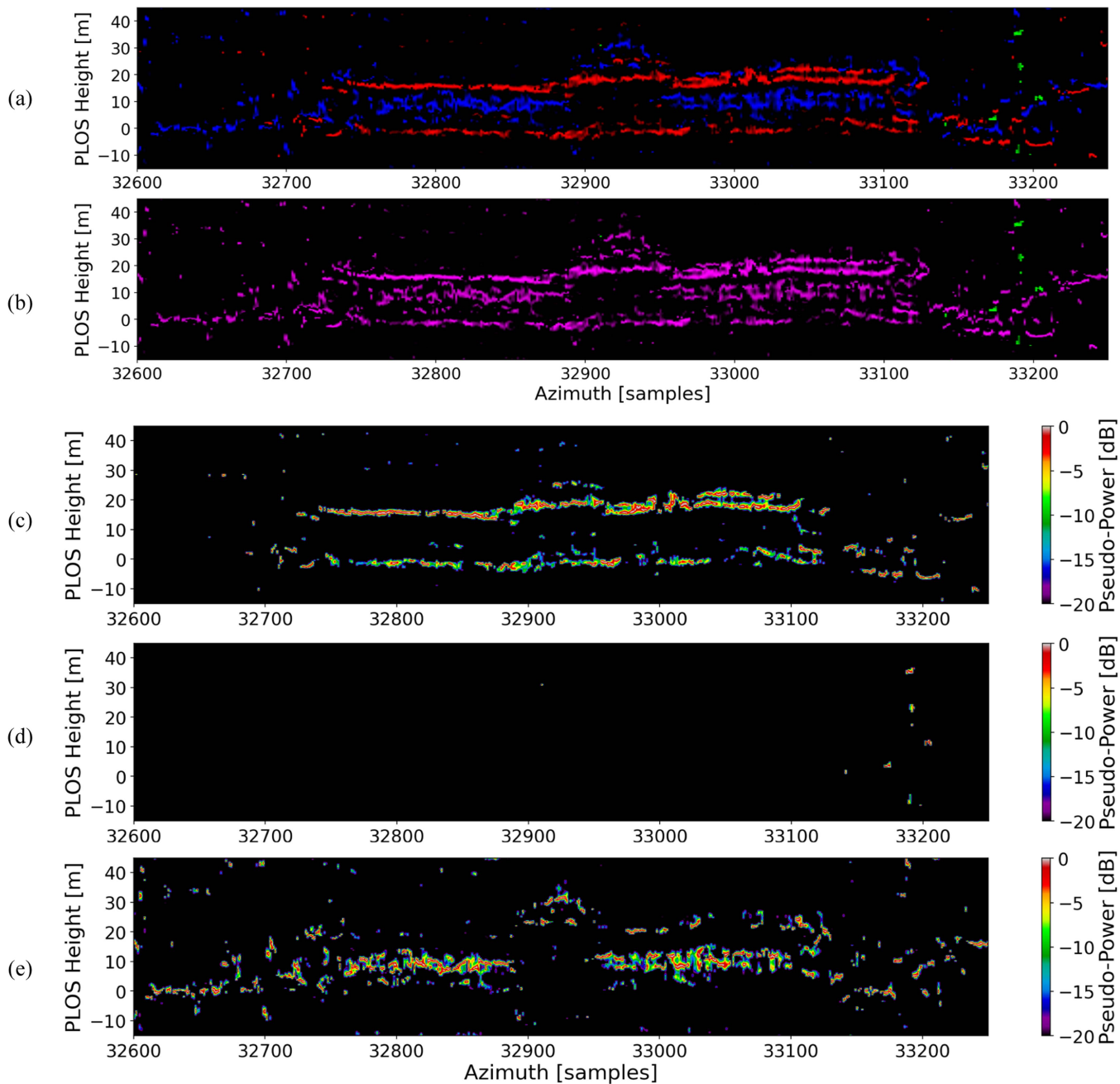
Fig. 23.　PolWISE tomograms from the ROI in Fig. 19. (a) Lexicographic [Red (first Channel), Green (second Channel), Blue (third Channel)]. (b) Pauli. (c) First Channel: double-bounce reflection. (d) Second Channel: volume scattering. (e) Third Channel: singles-bounce reflection.
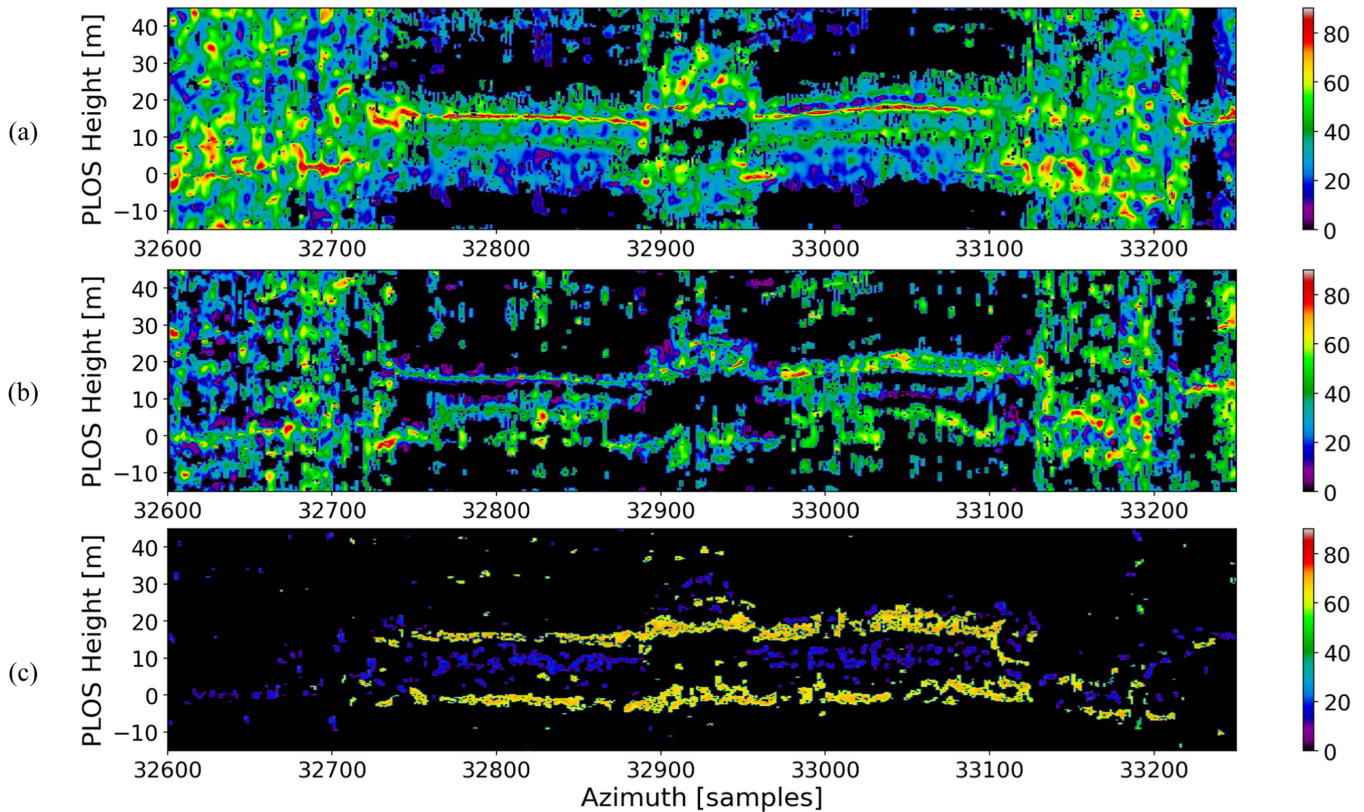
Fig. 24. Bavarian state chancellery: alpha mean angle $\bar{\alpha}$ in degrees. (a) PolCapon. (b) PolMUSIC. (c) PolWISE.

VIII. CONCLUSION

This article introduces PolWISE, a super-resolution technique, which reduces the WCF optimization problem to the selection of a regularization parameter. When such regularization parameter is chosen appropriately, by instance, via L-Curve method, PolWISE provides good-fitted results. PolWISE attains finer resolution given lower resolution imagery, obtained, for example, using PolCapon. Furthermore, it also achieves ambiguity reduction and artefacts suppression. These enhancements facilitate the estimation of the height of reflectors (one of the main goals of TomoSAR) and the analyses of the scattering processes occurring in the illuminated scene.

PolWISE is an iterative approach, which holds higher computational complexity than conventional techniques like PolCapon and PolWISE. Moreover, the number of iterations required to converge increases with the number of channels, augmenting processing time. Therefore, the usage of a stopping rule (e.g., AIC, BIC, and EDC) is recommended to terminate the iterative procedure immediately after convergence is reached. This also prevents under/over regularization due to wrong number of iterations.

PolWISE performs better in urban scenarios characterized by point-type like targets. More SNR is needed to discern the phase-centers of distributed targets. For the full channel simulated scenario in Table I, SNR above 20 dB is required to discriminate all phase-centers. For lower SNR, PolWISE treats some distributed targets as noise, suppressing them.

PolWISE results split into three channels: the first channel refers to double bounce-reflection, the second channel to volume reflection, and the third channel to single-bounce reflection. The pseudopower profiles of each channel complement each other but do not overlap. Thanks to the characteristics of PolWISE, it is easier to label the locations of certain type of scattering mechanism by computing, for example, the polarimetric indicator alpha mean angle $\bar{\alpha}$. Nonetheless, we suggest treating PolWISE results as complementary information, since some information might be filtered out.

REFERENCES

[1] S. R. Cloude and E. Pottier, "A review of target decomposition theorems in radar polarimetry," *IEEE Trans. Geosci. Remote Sens.*, vol. 34, no. 2, pp. 498–518, Mar. 1996.

[2] S. R. Cloude and E. Pottier, "An entropy-based classification scheme for land applications of polarimetric SAR," *IEEE Trans. Geosci. Remote Sens.*, vol. 35, no. 1, pp. 68–78, Jan. 1997.

[3] P. A. Rosen et al., "Synthetic aperture radar interferometry," *Proc. IEEE*, vol. 88, no. 3, pp. 333–382, Mar. 2000.

[4] G. Krieger et al., "TanDEM-X: A satellite formation for high-resolution SAR interferometry," *IEEE Trans. Geosci. Remote Sens.*, vol. 45, no. 11, pp. 3317–3341, Nov. 2007.

[5] A. Reigber and A. Moreira, "First demonstration of airborne SAR tomography using multibaseline L-band data," *IEEE Trans. Geosci. Remote Sens.*, vol. 38, no. 5, pp. 2142–2152, Sep. 2000.

[6] S. R. Cloude and K. P. Papathanassiou, "Polarimetric SAR interferometry," *IEEE Trans. Geosci. Remote Sens.*, vol. 36, no. 5, pp. 1551–1565, Sep. 1998.

[7] S. Sauer, L. Ferro-Famil, A. Reigber, and E. Pottier, "Three-dimensional imaging and scattering mechanism estimation over urban scenes using dual-baseline polarimetric InSAR observations at L-band," *IEEE Trans. Geosci. Remote Sens.*, vol. 49, no. 11, pp. 4616–4629, Nov. 2011.

[8] G. Martín del Campo, M. Nannini, and A. Reigber, "Statistical regularization for enhanced TomoSAR imaging," *IEEE J. Sel. Topics Appl. Earth Observ. Remote Sens.*, vol. 13, pp. 1567–1589, 2020.

[9] G. D. Martín-del-Campo-Becerra, S. A. Serafín-García, A. Reigber, and S. Ortega-Cisneros, "Parameter selection criteria for Tomo-SAR focusing," *IEEE J. Sel. Topics Appl. Earth Observ. Remote Sens.*, vol. 14, pp. 1580–1602, 2021.

[10] A. Cultrera and L. Callegaro, "A simple algorithm to find the L-curve corner in the regularization of inverse problems," *IOP SciNotes*, vol. 1, no. 2, pp. 1–6, Aug. 2020.

[11] P. Stoica and Y. Selen, "Model-order selection: A review of information criterion rules," *IEEE Signal Process. Mag.*, vol. 21, no. 4, pp. 36–47, Jul. 2004.

[12] G. D. Martín-del-Campo-Becerra, S. A. Serafín-García, A. Reigber, S. Ortega-Cisneros, and M. Nannini, "Resolution enhancement of spatial parametric methods via regularization," *IEEE J. Sel. Topics Appl. Earth Observ. Remote Sens.*, vol. 14, pp. 11335–11351, 2021.

[13] P. Stoica and R. L. Moses, *Spectral Analysis of Signals*, vol. 1. Upper Saddle River, NJ, USA: Prentice-Hall, 2005.

[14] F. Gini, F. Lombardini, and M. Montanari, "Layover solution in multibaseline SAR interferometry," *IEEE Trans. Aerosp. Electron. Syst.*, vol. 38, no. 4, pp. 1344–1356, Oct. 2002.

[15] H. H. Barrett and K. J. Myers, *Foundations of Image Science*. New York, NY, USA: Willey, 2004.

[16] M. Nannini, R. Scheiber, and A. Moreira, "Estimation of the minimum number of tracks for SAR tomography," *IEEE Trans. Geosci. Remote Sens.*, vol. 47, no. 2, pp. 531–543, Feb. 2009.

[17] M. Schmitt and U. Stilla, "Maximum-likelihood-based approach for single-pass synthetic aperture radar tomography over urban areas," *IET Radar, Sonar Navigation*, vol. 8, no. 9, pp. 1145–1153, Apr. 2014.

[18] F. Lombardini and F. Viviani, "Radiometrically robust superresolution tomography: First analyses," in *Proc. IEEE Int. Geosc. Remote Sens. Symp.*, 2016, pp. 24–27.

[19] P. Stoica, P. Babu, and J. Li, "New method of sparse parameter estimation in separable models and its use for spectral analysis of irregularly sampled data," *IEEE Trans. Sign. Process.*, vol. 59, no. 1, pp. 35–47, Jan. 2011.

[20] P. Stoica, P. Babu, and J. Li, "SPICE: A sparse covariance-based estimation method for array processing," *IEEE Trans. Sign. Process.*, vol. 59, no. 2, pp. 629–638, Feb. 2011.

[21] J. L. Mueller and S. Siltanen, *Linear and Nonlinear Inverse Problems With Practical Applications*, vol. 10. Philadelphia, PA, USA: SIAM, 2012.

[22] F. Lombardini and F. Gini, "Model order selection in multi-baseline interferometric radar systems," *EURASIP J. Adv. Signal Process.*, vol. 2005, no. 20, pp. 3206–3219, 2005.

[23] S. Hensley et al., "UAVSAR Tomography of Munich," in *Proc. IEEE Int. Geosci. Remote Sens. Symp.*, 2019, pp. 1140–1143.

[24] C. E. Jones, B. Minchew, B. Holt, and S. Hensley, "Studies of the Deepwater Horizon oil spill with the UAVSAR radar," in *Monitoring and Modeling the Deepwater Horizon Oil Spill: A Record-Breaking Enterprise*, Y. Liu, A. MacFadyen, Z.-G. Ji, and R. H. Weisberg, Eds. Washington, DC, USA, Aug. 2011, pp. 33–50.

[25] J. S. Lee and E. Pottier, *Polarimetric Radar Imaging: From Basics to Applications*. Boca Raton, FL, USA: CRC, 2017.

[26] E. T. F. Santos and A. Bassrei, "L-and Θ-curve approaches for the selection of regularization parameter in geophysical diffraction tomography," *Comput. Geosciences*, vol. 33, no. 5, pp. 618–629, May 2007.

Eduardo Torres-García received the Engineering degree in telematics from the Polytechnic University of Juventino Rosas, Guanajuato, Mexico, in 2020, and the M.Sci. degree in electrical engineering in 2022 (*with specialization in telecommunications*) from the Center for Research and Advanced Studies (Cinvestav), National Polytechnic Institute, Guadalajara, Mexico, where he is currently working toward the Dr.Sci. (Ph.D. equivalent) degree in electrical engineering.

His research interests include the applications of signal processing to remote sensing, specifically, SAR tomography (TomoSAR), and Polarimetric SAR (PolSAR).

Deni Librado Torres-Román received the Ph.D. degree in telecommunication from the Technical University Dresden, Dresden, Germany, in 1986.

He was a Professor with the University of Oriente, Cuba. He has been a Researcher 3-C with CINVESTAV- IPN, Guadalajara, Mexico, since 1996. He has coauthored a book about data transmission. His research interests include hardware and software design for applications in the telecommunication area.

Prof. Deni was the recipient of the Telecommunication Research Prize in 1993 from AHCIET Association and the 1995 Best Paper Award from AHCIET Review, Spain. In recent years, he is working with tensor algebra for MS- and HS-Imaging, and video processing.

Sergio Alejandro Serafín-García received the Engineering degree in electronics and communications engineering from the University of Guadalajara, Guadalajara, Mexico, in 2017, and the M.Sci. degree in electrical engineering (*with specialization in telecommunications*) from the Center for Research and Advanced Studies (Cinvestav), National Polytechnic Institute, Guadalajara, Mexico, in 2021. He is currently working toward the Ph.D. degree with the Microwaves and Radar Institute (HR), German Aerospace Center (DLR).

His research interests include the applications of signal processing and machine learning to remote sensing, particularly SAR tomography (TomoSAR).

Gustavo Daniel Martín-del-Campo-Becerra received the Engineering degree in electronics and communications engineering from the University of Guadalajara, Guadalajara, Mexico, in 2008, and the M.Sci. and Dr.Sci. (Ph.D. equivalent) degrees in electrical engineering (*with specialization in telecommunications*) from the Center for Research and Advanced Studies (Cinvestav), National Polytechnic Institute, Guadalajara, Mexico, in 2013 and 2017, respectively.

Since 2017, he has been with the Microwaves and Radar Institute (HR), German Aerospace Center (DLR), as a Research Scientist. His research interests include the applications of signal processing and machine learning to remote sensing, particularly SAR tomography (TomoSAR), inverse problems, random fields estimation, and adaptive spatial analysis.

Andreas Reigber (Fellow, IEEE) received the Diploma degree in physics from the University of Konstanz, Konstanz, Germany, in 1997, the Ph.D. degree in engineering from the University of Stuttgart, Stuttgart, Germany, in 2001, and the Habilitation degree from the Berlin University of Technology, Berlin, Germany, in 2008.

He is currently the Head of the SAR Technology Department, Microwaves and Radar Institute (HR), German Aerospace Center (DLR), Weßling, Germany, where he is leading the development and operation of state-of-the-art airborne SAR sensors. He is also a Professor of remote sensing and digital image processing with the Berlin University of Technology, Berlin, Germany. His research interests include various aspects of multimodal, multichannel, and high-resolution SAR processing and postprocessing.

Dr. Reigber was the recipient of several prize paper awards, among them the IEEE TRANSACTIONS ON GEOSCIENCE AND REMOTE SENSING (IEEE TGRS) Prize Paper Award in 2001 and 2016 for his works on polarimetric SAR tomography and nonlocal speckle filtering, respectively, and also the IEEE TGRS Letters Prize Paper Award in 2006 for his work on multipass SAR processing.